nature reviews materials

https://doi.org/10.1038/s41578-024-00755-1

Review article

Check for updates

Non-faradaic junction sensing

Yecheng Wang [1] ✉, Kun Jia [2] ✉ & Zhigang Suo [3] ✉

Abstract

A non-faradaic junction (NFJ) is a connection between an ionic conductor and an electronic conductor in which no electrochemical reaction takes place. The junction behaves like a capacitor and couples the ionic and electronic currents through chemistry, electricity and entropy. Its charge–voltage curve is sensitive to various environmental signals, allowing it to function as a sensor; because no reaction occurs, the sensing is non-destructive and long-lasting. NFJ sensors have high sensitivity, rapid response and small size, and they can be self-powered. These sensors are familiarly used in electrophysiology of the heart, brain and muscles, and applications are emerging in wearable and implantable devices and soft robotics, as well as in sensing pressure, sound, temperature and chemicals. In this Review, we discuss NFJ sensors, emphasizing the development of devices and materials for each side of the junction. The flexibility in choosing materials enables NFJ sensors to fulfil challenging requirements, such as softness, stretchability, transparency and degradability.

Sections

Introduction

Principles of non-faradaic junction sensing

Characterization of junctions by voltage steps

Pressure sensing

Acoustic sensing

Temperature sensing

Chemical sensing

Materials

Outlook

[1]Guangdong Provincial Key Laboratory of Magnetoelectric Physics and Devices, School of Physics, Sun Yat-sen University, Guangzhou, China. [2]State Key Laboratory for Strength and Vibration of Mechanical Structures, Department of Engineering Mechanics, Xi'an Jiaotong University, Xi'an, China. [3]John A. Paulson School of Engineering and Applied Sciences, Kavli Institute for Bionano Science and Technology, Harvard University, Cambridge, MA, USA. ✉e-mail: wangych286@mail.sysu.edu.cn; kunjia@mail.xjtu.edu.cn; suo@seas.harvard.edu

Introduction

We live in a world of ceaseless signals, which enable people, animals and plants to perceive the world through sensors. For example, a sunflower detects the sun via photoreceptors, and animals and people sense temperature, pressure and smell via sensory neurons. A vision has emerged that artificial intelligence should also perceive the world through sensors. To apply artificial intelligence to personalized health care, for example, many signals must be measured from many people to train models and then suggest medical decisions for individuals[1]. This requirement calls for the development of ubiquitous sensing technologies.

Computers function through electronic circuits and rely on electronic conductors. Humans function through ionic circuits and are mostly ionic conductors. It is perhaps no surprise that many health-monitoring sensors involve both electronic conductors and ionic conductors, coupling the movement of electrons in the computers with the movement of ions in the living tissues. Although several reviews have described sensors that integrate electronic and ionic conductors[2–8], this Review focuses on sensors built on the following principle: junctions of electronic conductors and ionic conductors are sensitive to environmental signals.

In such a junction, the electronic conductor is called an electrode, and the ionic conductor is called an electrolyte. An electrode–electrolyte junction is faradaic if an electrochemical reaction takes place. For example, a hydrogen fuel cell has two electrode–electrolyte junctions[9]. At one junction, hydrogen molecules decompose into protons and electrons. At the other junction, the protons, electrons and oxygen molecules react to form water. In addition to fuel cells, faradaic junctions have found applications in batteries[10] and electrochemical sensors[11].

By contrast, an electrode–electrolyte junction is non-faradaic if no electrochemical reaction takes place. At a non-faradaic junction (NFJ), electrons in excess or deficiency are trapped at the interface, and some species of ions adsorb to the interface more than others. The trapped electrons and the adsorbed ions together constitute the interfacial charge, which in general is not neutral. To compensate for the interfacial charge, an ionic atmosphere forms in the interior of the electrolyte. The interface and the ionic atmosphere together constitute the NFJ, which functions like a capacitor. NFJs have found applications in supercapacitors[12], sensors[11] and actuators[13].

An NFJ is sensitive to environmental signals, such as pressure, acoustic waves, temperature and chemicals, making it an ideal platform for sensing. Because the interface is not charge-neutral, the junction is a pre-charged capacitor, and an NFJ sensor can be made self-powered. Because the thickness of the junction is small, ~1–10 nm, ions only need to diffuse over small distances, and an NFJ sensor is fast. Because the capacitance of the junction is large, ~0.1 F m^{-2} (ref. 14), an NFJ sensor is sensitive and can be made small. Because no reaction takes place, the junction does not produce or consume chemical species in large quantities, and an NFJ sensor can be made long-lasting.

NFJ sensing has long been practised in electrophysiology, which monitors physiological conditions by turning ionic movements in tissues to electronic currents in computers. Tissues monitored include the heart (electrocardiology), the brain (electroencephalography) and the muscle (electromyography). However, electrophysiology traditionally requires people to be connected to computers through wires and hard, bulky and immobile devices, limiting the scope of applications. Sensing technologies are transitioning to wireless, wearable and implantable devices, which must be soft, small and mobile to enable continuous, real-time, on-the-go monitoring[15–22]. To meet these demands, a newer generation of NFJ sensors must be developed.

In this Review, we discuss the development of sensors based on NFJs. We begin with the principle of NFJ sensing and the basic electric circuits for calibrating and operating the sensors. We then describe sensors of several types of signals, including pressure, sound, temperature and chemicals. We summarize the materials used to make the sensors, including the electronic conductor, ionic conductor and dielectric, and discuss how the flexibility in choosing these materials enables NFJ sensors to fulfil challenging requirements, such as softness, stretchability, transparency and degradability. We end with an outlook on the challenges and opportunities in this field.

Principles of non-faradaic junction sensing

Consider an interface between an electrolyte and an electrode (Fig. 1a). Some species of ions in the electrolyte adsorb to the interface more than others. The electrons in the electrode are in excess or deficiency at the interface. In general, the interface is not electroneutral. The interior of the electrode has a high density of mobile electrons and is therefore electroneutral. The interior of the electrolyte has a low density of mobile ions. The charged interface attracts ions of the opposite polarity and repels ions of the same polarity. Far away from the interface, the electrolyte is electroneutral.

To gain physical insight into an NFJ, we examine an idealized model[14]. In the electrolyte, the mobile ions increase entropy by dispersing homogeneously, but the charged interface reduces electrostatic energy by attracting ions of the opposite polarity and repelling ions of the same polarity. In equilibrium, the two competing effects — entropy and electroneutrality — cause the mobile ions in the electrolyte to form an atmosphere near the interface. The ionic atmosphere is charged and has the opposite polarity from the interface. The thickness of the ionic atmosphere is called the Debye length[14]:

$$L = \sqrt{\frac{\varepsilon kT}{n^{+}(\infty)\nu^{+}(\nu^{+} + \nu^{-})e^{2}}} \quad (1)$$

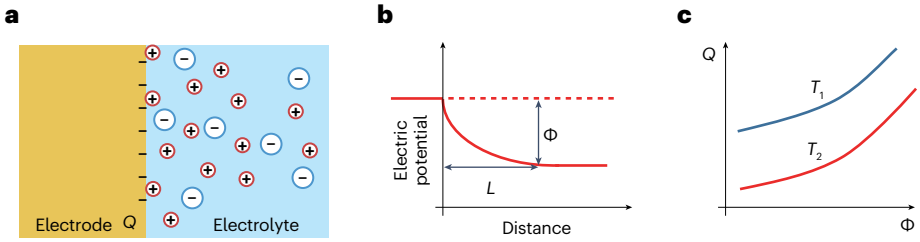

Fig. 1 | Principles of non-faradaic junction sensing. a, A non-faradaic junction. **b**, In the electrolyte, the electric potential varies with the distance from the interface. **c**, A non-faradaic junction behaves like a capacitor. The charge is a function of voltage and temperature, $Q(\Phi, T)$, represented by charge–voltage curves at various temperatures. The charge–voltage curves are used to sense temperature.

in which ε is the permittivity of the electrolyte, k is the Boltzmann constant, T is the temperature, $n^+(\infty)$ is the number density of the positive ions in the electrolyte far away from the interface, ν^+ and ν^- are the valences of positive and negative ions and e is the elementary charge. Beyond the Debye length, the electrolyte approaches electroneutrality.

By an NFJ, we mean the combination of the electrode–electrolyte interface and the ionic atmosphere. The combined charges on the interface and in the ionic atmosphere are electroneutral. The junction behaves like a capacitor, with a thickness scaled by the Debye length. As noted earlier, the chemistry of the interface makes the capacitor charged, even in the absence of an external power source. Let Q be the charge on the interface:

$$Q = \sigma A, \tag{2}$$

in which σ is the charge density at the electrode–electrolyte interface, including both the electrons and ions, and A is the area of the interface.

In equilibrium, the electrode has one constant electric potential, and the bulk of the electrolyte at a distance much beyond the Debye length has another constant electric potential (Fig. 1b). The difference between these two constant electric potentials is the voltage across the junction, Φ. The junction voltage relates to the interfacial charge and the Debye length as

$$\Phi = \frac{\sigma}{\varepsilon} L. \tag{3}$$

The charge–voltage curve of an NFJ is sensitive to environmental signals and can be used as a sensor. To illustrate the principles of NFJ sensing, consider temperature sensing. As noted earlier, electroneutrality and entropy compete to set up the ionic atmosphere. At a low temperature, electroneutrality prevails, the mobile ions in the electrolyte migrate to the interface to neutralize the charged interface and the ionic atmosphere collapses. At a high temperature, entropy prevails, and the ionic atmosphere expands. A change in temperature typically also changes the amount of adsorbed ions and trapped electrons at the interface. Consequently, when temperature T changes, so also changes the voltage across the junction Φ. In general, the charge on the interface is a function of the voltage and temperature: $Q(\Phi, T)$ (Fig. 1c). Given a junction, this function can be determined experimentally by measuring the charge–voltage curves at various temperatures. The junction can then operate as a temperature sensor.

According to equation (1), the Debye length also depends on the concentration and type of ions, as well as on the type of solvent. Moreover, the type of electrode affects the interfacial charge. Consequently, the voltage across the junction depends on the concentration and type of ions, as well as on the type of solvent and electrode. All these factors can affect NFJ sensing. One may deliberately choose the electrolyte and electrode to achieve high sensitivity, rapid response and long-term stability simultaneously.

Characterization of junctions by voltage steps

Although illustrated above using temperature sensing, the principle of NFJ sensing is applicable to many types of signals, including pressure, sound and chemicals. Because the charge–voltage curve of an electrode–electrolyte junction is sensitive to many signals, a sensor of a given signal can be built once it is determined how the signal affects the charge–voltage curve. A charge–voltage curve is determined by experimental measurements when the levels of signals are held constant.

To characterize junctions, as an example setup, two gold electrodes are immersed in an aqueous solution of 1 M sodium chloride (Fig. 2a). The two electrodes are connected through an external circuit to a power source, a voltmeter and an ammeter. Before the power source is turned on, the two electrodes are immersed in the electrolyte for a sufficiently long time to reach equilibrium, where the voltmeter reads a voltage independent of time and the ammeter reads negligible current. At time t_0, a power source (such as a Keithley 2400 instrument) applies a voltage step (Fig. 2b) and records the current as a function of time (Fig. 2c). The applied voltage is

$$V = \Phi_1 - \Phi_2, \tag{4}$$

in which Φ_1 and Φ_2 are the voltages across the two junctions, respectively. When the junctions are faradaic, an electrochemical reaction takes place, and after some time the current approaches a steady state. When the junctions are non-faradaic, no electrochemical reaction takes place, and after some time the current vanishes. In reality, a small leakage current may exist, and the junctions are taken to be non-faradaic if the steady-state current is below a certain small value, say, 1 μA cm^{-2}. The area under the current–time curve gives the charge flowing through the external circuit (Fig. 2d). As an idealization, we neglect the small leakage and approximate the equilibrium charge by the charge measured within a certain time, say, 15 s.

One then applies voltage in a sequence of steps. For each voltage step, one measures a steady-state current. On the current–voltage plane, the voltage applied and the steady-state current correspond to a point (Fig. 2e). Once the voltage steps are small enough, the points on the current–voltage plane may be connected as a smooth curve, called the I–V curve. The steady-state current is non-zero when the junctions are faradaic, but it is approximately zero when the junctions are non-faradaic. Often, the junctions are non-faradaic when the voltage is within a range called the electrochemical window. The electrochemical window is the difference between the two electrode potentials when the setup is subject to a static voltage, and is constant for given junctions. Outside the electrochemical window, the junctions are faradaic. The I–V curve loses the information of the time needed to reach steady-state current for each voltage step. The I–V curve can also be measured by a voltage ramping up as a function of time, so long as the ramping rate is low enough.

One measures the electronic current in the external circuit. Over a time, the measured current gives a change in charge. For an NFJ, this change in the electronic charge is fully accumulated at the interface. One can increase the voltage in a sequence of steps and measure an equilibrium charge for each voltage step. A voltage step and its corresponding equilibrium charge mark a point on the charge–voltage plane (Fig. 2f). Once the voltage steps are small enough, the points on the charge–voltage plane may be connected as a smooth curve, called the Q–V curve. In addition to voltage steps, other voltage–time curves may be applied to characterize junctions. Widely used methods include voltage ramps[14] and cyclic voltammetry[23].

Pressure sensing

NFJs have been widely applied to sense pressure and touch[24–29]. An NFJ pressure sensor consists of a soft, elastic, ionic conductor sandwiched between two electronic conductors (Fig. 3a). At each interface between

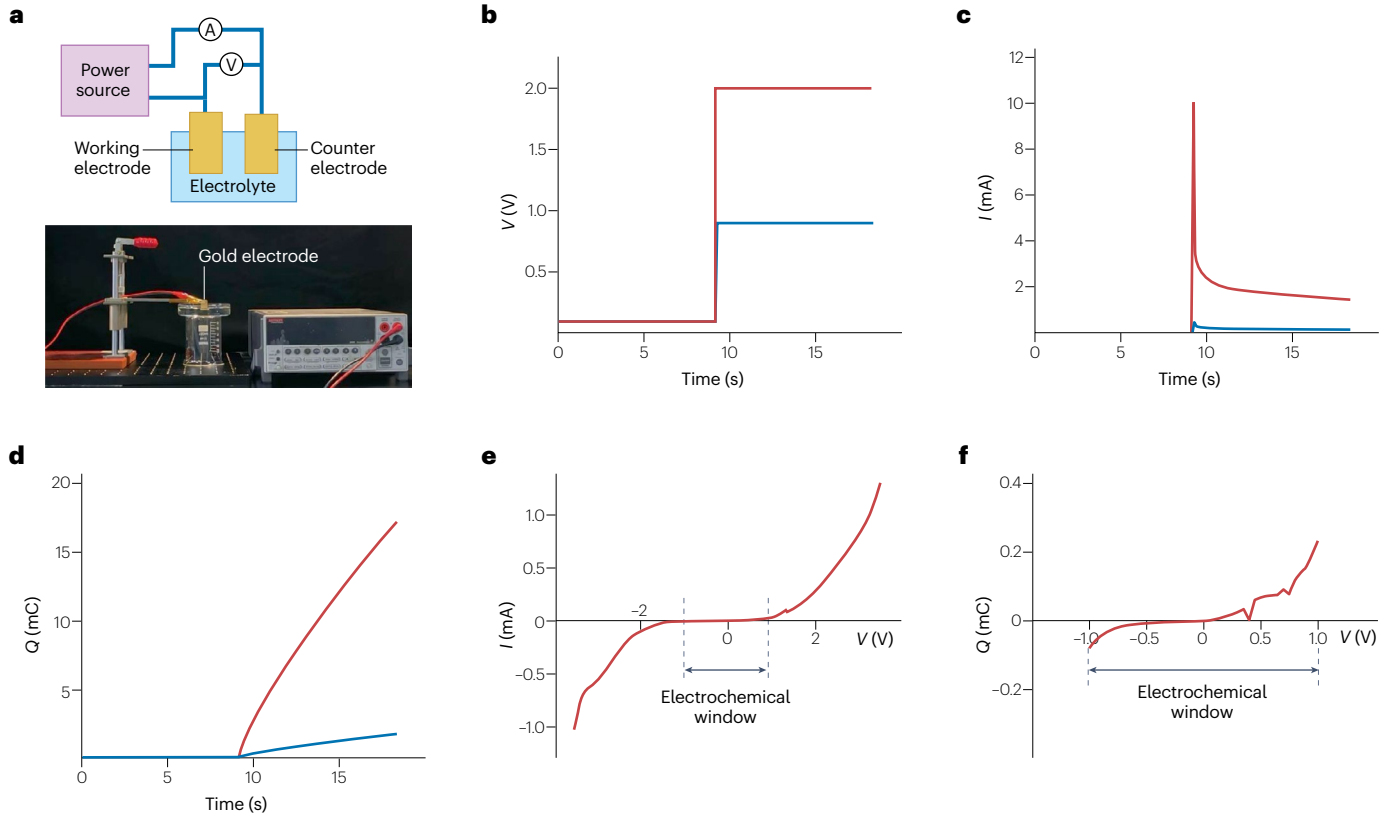

Fig. 2 | Characterization of two electrodes in an electrolyte by a sequence of voltage steps. a, The experimental setup. In this example, both electrodes are gold and the electrolyte is an aqueous solution of sodium chloride of concentration 1 M. **b**, The power source is programmed to apply two voltage steps indicated by the red and blue lines. **c**, The ammeter records the current as a function of time for the two voltage steps. The area under the current–time curve gives the charge flowing across the ammeter. **d**, The charge is a function of time. **e**, The relation between steady-state current and voltage. **f**, The relation between equilibrium charge and voltage.

the ionic and electronic conductors, an NFJ forms. Under compression, the soft ionic conductor deforms, increasing the contact area between the electronic conductor and the ionic conductor and increasing the capacitance of the junction (Fig. 3b). NFJ pressure sensors have high sensitivity, high resolution and broad detection range. So long as the ionic conductor is elastic, the deformation can be repeated for many cycles.

Each electrode–electrolyte junction is represented by a capacitor C_I in parallel with a leakage resistor R_I (Fig. 3c). The electrolyte is represented by a resistor R_B. An LCR metre is widely used to measure the capacitance of the pressure sensor. The LCR metre applies a sinusoidal voltage within the electrochemical window and measures a sinusoidal current. The ratio of the voltage amplitude and current amplitude determines the magnitude of the impedance of the pressure sensor. The phase angle between the voltage and the current determines the phase of the impedance of the pressure sensor. To determine the capacitance of the sensor, the LCR metre should be incorporated by an electric circuit model for the pressure sensor.

The impedance is

$$Z = R_B + \frac{2R_I}{(1 + j\omega C_I R_I)}, \quad (5)$$

in which $\omega = 2\pi f$ is the angular frequency and $j = \sqrt{-1}$. The leakage resistance is negligible if $R_B \gg \frac{2R_I}{(1+\omega^2 C_I^2 R_I^2)}$. The LCR metre measures R_B and C_I by fitting the function $Z(\omega)$ to the electric circuit model.

The sensitivity and detection range of the sensor can be enhanced by introducing microstructures to the electronic conductor[30–32] or to the ionic conductor[33–41], so that the contact area further increases under pressure. Examples of such structures include micropyramids[33,39–41] (Fig. 3d), nanofibrous structures[34] (Fig. 3e), microstructures of different heights[35] (Fig. 3f), microgrooves[36] (Fig. 3g), multilayered microstructures[37] (Fig. 3h) and hemispheres with micropillars[38] (Fig. 3i). A sensor incorporating an array of pyramidal ionogels can detect pressure from a lightweight flower (4 Pa), jugular venous pulses (2 kPa), radial artery pulses (4 kPa) and the touch of a human finger (<10 kPa)[33] (Fig. 3d). A sensor of microstructures of different heights can detect a pressure of about 1 Pa (ref. 35) (Fig. 3f). A sensor of microgrooves can detect a pressure below 0.1 Pa (ref. 36) (Fig. 3g). The junction capacitance is proportional to the contact area, but the contact area can be nonlinear in pressure. Consequently, the sensitivity is pressure-dependent and usually decreases at large pressure.

NFJ pressure sensors with high resolution and broad detection range have been used for cardiovascular pressure measurement[24,25]. An NFJ pressure sensor attached to the skin above the carotid or radial

artery is able to monitor the variations of blood pressure. In the measurement, the sensor should be gently pressed to the neck or fixed with a plastic wristband. An array of pressure sensors are also able to map the static surface topology[25] or work for tactile perception[31,34].

Several other types of pressure sensors — including piezoelectric, piezoresistive, capacitive and triboelectric — are also under development for wearable applications. NFJ pressure sensors can be viewed as a class of capacitive sensors, of thickness scaled by the Debye length. However, because of large junction areas and small junction thicknesses, as well as high permittivity of electrolyte, NFJ pressure sensors have unusually large capacitance per unit area and can be made compact. Consequently, they can typically detect smaller pressures than other capacitive pressure sensors. For piezoelectric pressure sensors, only certain materials that possess electric dipoles can be selected. For NFJ pressure sensors, many materials can be selected, as long as no electrochemical reaction occurs. In addition, NFJ pressure sensors can detect static pressure, whereas piezoelectric and triboelectric pressure sensors cannot.

Acoustic sensing

NFJs have also been used to detect underwater acoustic waves of a broad frequency range. In one type of NFJ acoustic sensor, metal

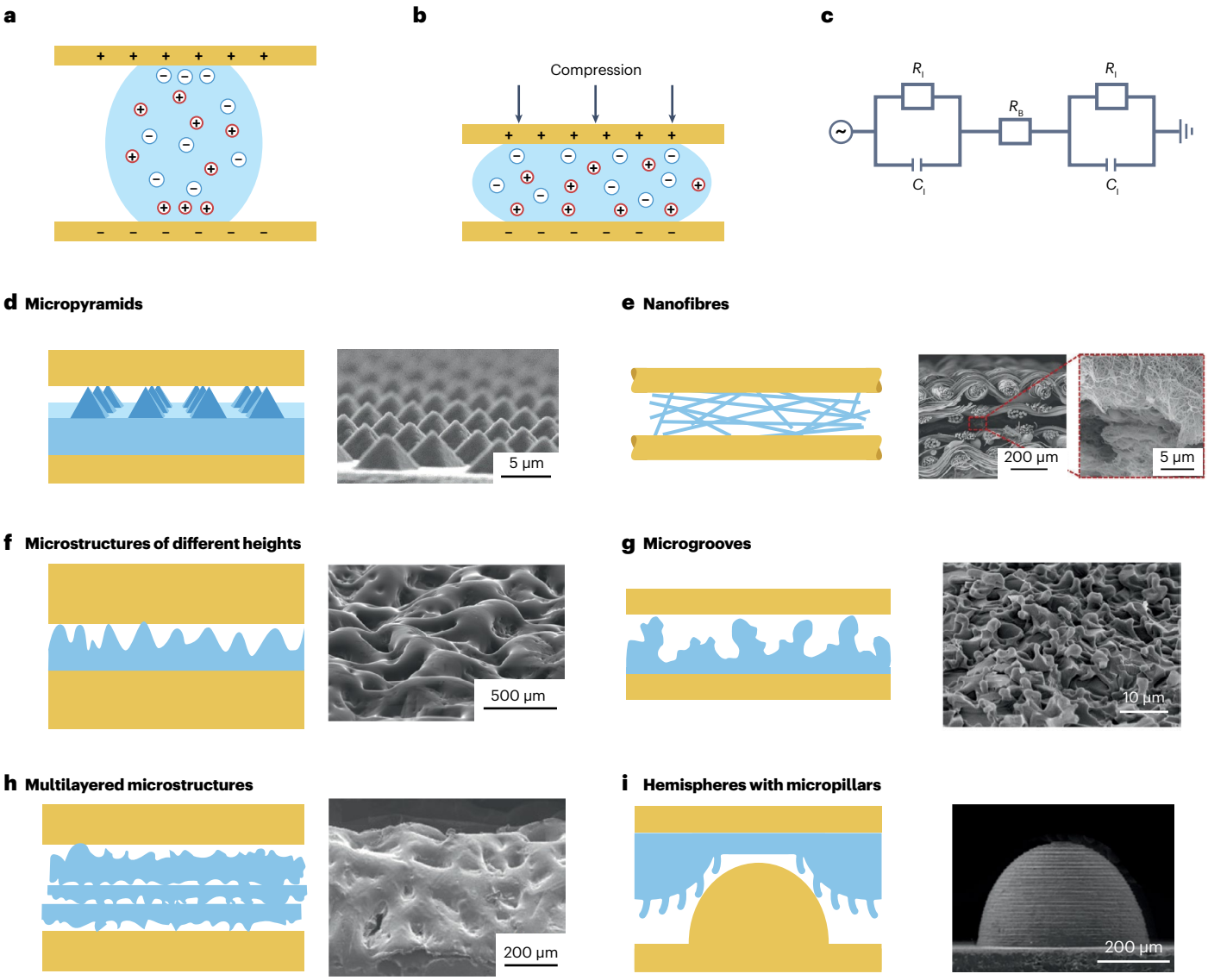

Fig. 3 | Non-faradaic junction pressure sensing. a, The sensing element consists of a soft, elastic, ionic conductor sandwiched between two electronic conductors. Each junction between the ionic conductor and the electronic conductor functions as a capacitor. **b**, When the sensing element is compressed, the area of the soft ionic conductor increases, and the capacitance of the junctions increases. **c**, Electric circuit model. **d**–**i**, To enhance the sensitivity, diverse microstructures are designed: micropyramids (part **d**)[33], nanofibrous structures (part **e**)[34], microstructures of different heights (part **f**)[35], microgrooves (part **g**)[36], multilayered microstructures (part **h**)[37] and hemispheres with micropillars (part **i**)[38]. Panel **d** adapted with permission from ref. 33, American Chemical Society. Panel **e** adapted with permission from ref. 34, Wiley. Panel **f** adapted with permission from ref. 35, American Chemical Society. Panel **g** adapted from ref. 36, CC BY 4.0. Panel **h** adapted with permission from ref. 37, American Chemical Society. Panel **i** adapted from ref. 38, American Chemical Society.

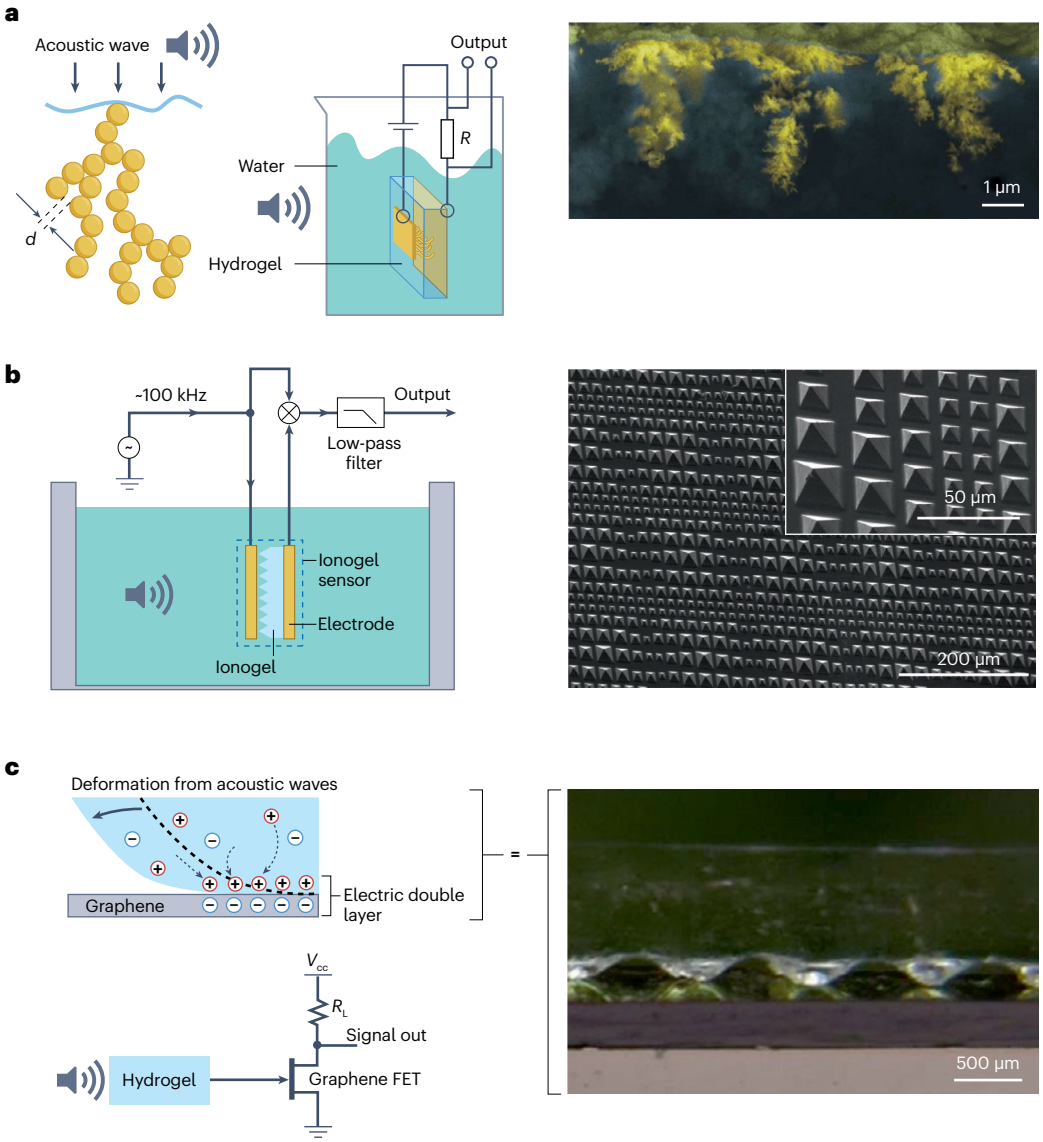

Fig. 4 | Non-faradaic junction acoustic sensing. a, Metal nanoparticle-incorporated hydrogel sandwiched between two electrodes[42]. The rigid nanoparticles form a network of dendritic structures, and junctions form between the nanoparticles and the hydrogel. In response to acoustic waves, the spacing between parts of the nanoparticle network changes, which affects the junction capacitance. **b**, Ionogel sandwiched between two electrodes[43]. In response to acoustic waves, the contact area between the ionogel and the electrode changes, which affects the junction impedance. On the surface of the ionogel are micropyramids, which further increase the contact area between the ionogel and the electrode. **c**, Hydrogel–graphene transistor[44]. Junctions form between a layer of graphene grown on a silicon channel and a hydrogel cast on top of the graphene. In response to the acoustic waves, the contact area between the hydrogel and the graphene changes, which affects the junction capacitance and the current flowing through the channel at a given gate voltage. On the surface of the hydrogel are also micropyramids, which further increase the contact area between the hydrogel and the graphene. FET, field-effect transistor. Panel **a** adapted from ref. 42, CC BY 4.0. Panel **b** adapted with permission from ref. 43, American Chemical Society. Panel **c** reprinted with permission from ref. 44, American Chemical Society.

nanoparticles embedded in a salt-containing hydrogel act as a deformable electrode[42] (Fig. 4a). The rigid nanoparticles form a network, and the hydrogel fills the spaces between them, creating junctions at the interfaces. Because the hydrogel is soft, the network of nanoparticles is flexible in response to acoustic waves. By design, the spacing between parts of the nanoparticle network is comparable to the Debye length, so that a change in the spacing affects the junction capacitance. This sensor can detect underwater acoustic signals from 20 Hz to 3 kHz at amplitude 4 Pa.

To understand the detection limits of this hydrogel sensor, picture two nanoparticles and the surrounding hydrogel as a mass–spring system, with mass ~ρd^3 and spring constant ~Gd. Here, ρ is

the mass density, d is the spacing and G is the elastic modulus. The resonant frequency is ~ $\sqrt{\frac{G}{\rho d^2}}$. For representative values of G = 10 kPa, $\rho = 10^4$ kg m^{-3} and $d = 10^{-8}$ m, this estimate gives a resonance frequency of the order of 10^8 Hz, which is much larger than the upper limit frequency of the device. We believe that it is the electric response, rather than the mechanical response of the capacitive sensor, that limits the upper response frequency. In the measurement, the sensor at bias of 1 V is connected in series to a resistor of 100 kΩ, and the voltage between the two ends of the resistor is measured. The capacitance is ~10 nF and the resistance of the resistor is 100 kΩ, so that the response time is ~10^{-3} s. This hydrogel acoustic sensor has high sensitivity of 217 nF kPa^{-1} or 24 mC N^{-1} at bias of 1 V.

Another type of NFJ acoustic sensor is made of an ionogel sandwiched between two electrodes[43] (Fig. 4b). On the surface of the ionogel are micropyramids, which further increase the contact area. The acoustic waves can be detected by measuring the change in the impedance of the junction caused by the change in the contact area between the electrode and the ionogel.

In addition, a hydrogel–graphene transistor has been developed as an NFJ acoustic sensor[44] (Fig. 4c). A monolayer of graphene is grown on a silicon channel and a hydrogel is cast on top of the graphene, forming junctions. The acoustic vibration changes the capacitance of the junctions, which in turn changes the current through the channel. By measuring the relation between the gate voltage and the channel current, one can detect the acoustic waves. To improve the sensitivity of the acoustic sensor, microstructures are introduced to the hydrogel to further increase the contact area between the hydrogel and the graphene.

NFJ acoustic sensors have higher sensitivity than traditional optical, piezoelectric and capacitive acoustic sensors at low frequency. For example, the hydrogel-based NFJ acoustic sensor described in Fig. 4a with a surface area of 9 mm^2 produces a signal 30 dB stronger at ~25 Hz than a commercial capacitive acoustic sensor (SQ 26 Cetacean Research Technology, Seattle, WA, USA)[42]. Furthermore, this hydrogel sensor is acoustically invisible, because its acoustic impedance is nearly identical to that of water.

Temperature sensing

Temperature affects many physical properties, and in principle a change in any of these properties can be used to measure temperature. This idea led to the development of NFJ temperature sensing[45]. Although we have discussed the principle of an NFJ temperature sensor earlier, we now expand on the design and additional details of a real sensor.

In addition to the electrode, electrolyte and electrode–electrolyte junction, a sensing unit may also contain a dielectric between the electrode and electrolyte (Fig. 5a). The dielectric prevents electrochemical reactions at the electrode–electrolyte interface, so it is only needed when the electrode is non-polarizable. In general, owing to the charge imbalance between adsorbed ions at the electrolyte–dielectric interface and trapped electrons at the electrode–dielectric interface, an ionic atmosphere forms in the electrolyte. According to equation (1), when temperature T changes, the thickness of the ionic atmosphere L (that is, the Debye length) also changes. By setting the electric potential of the electrolyte far away from the interfaces to be zero, a change in temperature causes a change in the voltage across the junction by

$$\Phi = \frac{\sigma_i + \sigma_e}{\varepsilon} L - \frac{\sigma_e}{\varepsilon_d} d. \quad (6)$$

Here, σ_i is the adsorbed ions per unit area at the electrolyte–dielectric interface, σ_e is the trapped electrons per unit area at the electrode–dielectric interface, ε_d is the permittivity of the dielectric and d is the thickness of the dielectric. The dielectric needs to be thin compared with the Debye length, so that the junction voltage is dominated by the first term on the right-hand side of equation (6).

The electrode, electrolyte and dielectric (if needed) can be arranged in various designs to meet requirements of different applications[45]. The sensor can be made stretchable, transparent and/or stable based on the materials used for each component. Unlike the NFJ pressure and acoustic sensors which operate by measuring the impedance, the NFJ temperature sensor operates by measuring open-circuit voltage and self-energizes. The sensitivity of the sensor depends on the type of the electrode and the concentration of ions, but not on stretch. In the most basic design, two electrodes are connected by an ionic conductor, forming two junctions that serve as a sensing end and a reference end (Fig. 5b). In such a design, the two electrodes are assumed to be ideally polarizable and no dielectric is used. The reference end is held at a known temperature T_{ref}. When the temperature of the sensing end T changes, both the charge on the interface and the Debye length L may change. These changes cause a change in voltage, which is recorded by the voltmeter. A high sensitivity of ~1 mV K^{-1} and fast response time of ~10 ms are achieved. The asymmetry in the two junctions is crucial for sensing. When the electrodes at the sensing end and the reference end are identical, the voltages across the two junctions cancel out and do not respond to temperature.

In a second design, the sensing end has a stretchable electronic conductor (silver-plated fabric) and a stretchable ionic conductor (hydrogel) (Fig. 5c). A temperature difference between the sensing end and the reference end generates a voltage. As the silver nanoparticles on the fabric are rigid, stretch does not affect the junction. Consequently, the voltage is insensitive to stretch. This design enables a stretchable NFJ temperature sensor.

In a third design, the sensing end has a small piece of electronic conductor connected to two ionic conductors of different concentrations of ions, forming two asymmetric junctions (Fig. 5d). A stretchable and transparent dielectric elastomer is placed between the two ionic conductors for insulation. The three-layered structure serves as a stretchable and transparent interconnect between the sensing end and reference end. A temperature difference between the two ends generates a voltage, which is insensitive to stretch. This design enables a stretchable and transparent NFJ temperature sensor.

In a fourth design, the sensing unit has an ionic conductor sandwiched between two different electronic conductors, forming two asymmetric junctions (Fig. 5e). When the temperature of the sandwich changes, a voltage is generated. This design enables an NFJ temperature sensor without a reference end. When aluminium and gold are used as the two electronic conductors, a much higher sensitivity of ~10 mV K^{-1} and long-term stability are achieved. This is because a thin layer of native oxide exists on the surface of aluminium. The native oxide possesses hydroxyl groups, which enhance the adsorption of ions and thus the sensitivity. The thin layer of native oxide also serves as a dielectric, passivates the aluminium and stabilizes the sensor.

In the three latter designs, a stretchable and transparent dielectric elastomer (very high bond, VHB) is used for seal.

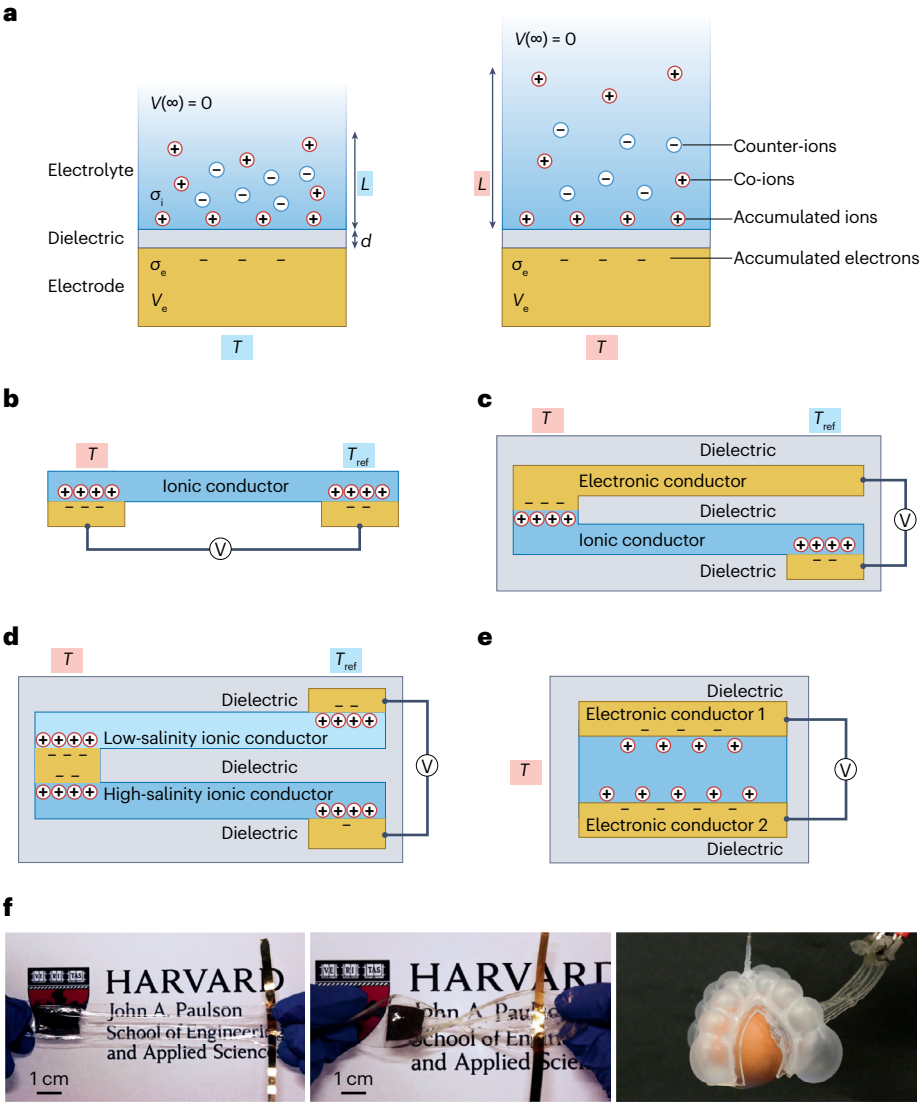

Fig. 5 | Non-faradaic junction temperature sensing. a, The sensing element consists of an electrode, an electrolyte and a dielectric, forming junctions. When temperature T changes from blue T to red T, the thickness of the ionic atmosphere L changes and the voltage across the junctions changes. **b**, Basic design. Two electrodes are connected by an ionic conductor, forming two junctions. When the temperature of one junction T changes and the temperature of the other junction is fixed at T_{ref}, an open-circuit voltage is generated. **c**, Stretchable design. A junction forms between a stretchable electrode and a stretchable ionic conductor, serving as the sensing end. The ionic conductor is connected to a voltmeter through another electrode, forming another junction as the reference end. A temperature difference between the two ends generates a voltage, which is insensitive to stretch. **d**, Stretchable and transparent design. A small piece of electrode is sandwiched between two ionic conductors of different concentrations of ions, forming two junctions as the sensing end. The two ionic conductors are connected to a voltmeter through another two electrodes, forming another junction as the reference end. A temperature difference between the sensing end and the reference end generates a voltage, which is insensitive to stretch. **e**, Design with no reference end. An ionic conductor is sandwiched between two different electrodes, forming two junctions. When temperature of the sandwich changes, a voltage is generated. Stretchable and transparent dielectric elastomers are used for seal and insulation in all designs. **f**, Stretchable and transparent non-faradaic junction temperature sensors for soft robots. Reprinted with permission from ref. 45, National Academy of Sciences.

The NFJ temperature sensor can be useful for applications in stretchable electronics, soft robots and smart textiles. For example, a stretchable and transparent NFJ temperature sensor has been integrated into a soft robot to accurately measure the temperature of curved surfaces (Fig. 5f). An NFJ of a polyelectrolyte and an electrode, in principle, can be also used as a temperature sensor, but remains unexplored.

We now discuss the electric circuit for open-circuit voltage measurement. Consider two electrodes connected by an electrolyte and a voltmeter (Fig. 5b). Each junction functions as a temperature-sensitive capacitor, and the voltmeter behaves like a resistor in series with an ammeter. The internal resistance of the voltmeter R_{volt} is large (typically above 10 MΩ), so that negligible current flows through the voltmeter.

When the change in charge is small, the junctions are approximately at equilibrium under the open-circuit condition. Consider two identical electrodes having the same charge Q. When both junctions are at the same temperature T_{ref}, the voltage across each junction is identical $\Phi(Q, T_{ref})$. Because the two junctions are in series with opposite polarities, the voltages of the two junctions cancel out, and the voltmeter records zero voltage. When the temperature of the sensing junction changes to T and the temperature of the reference junction is maintained at T_{ref}, the two junctions have the same charge Q, but the voltage across each junction is different, $\Phi(Q, T)$ and $\Phi(Q, T_{ref})$. As a result, the voltmeter records a voltage, $\Phi(Q, T) - \Phi(Q, T_{ref})$. The sensor is calibrated by measuring voltage–temperature curves.

To ensure reliable open-circuit measurement, the charge on the electrode should change negligibly. When the voltmeter records a voltage $\Phi(Q, T) - \Phi(Q, T_{ref})$, the charge flowing across the voltmeter during time t is $\frac{[\Phi(Q,T) - \Phi(Q,T_{ref})]t}{R_{volt}}$. For the representative values of $R_{volt} = 10$ MΩ, $\Phi(Q, T) - \Phi(Q, T_{ref}) = 10$ mV and $t = 10$ s, this estimate gives the charge flowing across the voltmeter 0.01 μC. Taking the voltage across a junction ~100 mV and the capacitance of a junction ~10 μF, we estimate that the charge of a junction is ~1 μC. Consequently, the charge flowing across the voltmeter is about 1% of the charge on the junction. To reduce the charge flowing across the voltmeter, a voltmeter of large

internal resistance and a junction of large capacitance are required. Large internal resistance decreases the current in the circuit, requires an ammeter of high sensitivity and increases the cost. Large junction capacitance can be realized by increasing the junction area.

Compared with a thermocouple[45], an NFJ temperature sensor offers a different way of measuring temperature. The NFJ sensor is based on an equilibrium thermodynamic phenomenon, but the thermocouple relies on non-equilibrium thermodynamic principles. In the NFJ sensor, the junction between the electrode and the electrolyte behaves like a capacitor, whereas the junction between two electrodes in the thermocouple conducts electricity. A change in temperature induces a transient current in the NFJ sensor but produces a steady current in the thermocouple. Both devices are self-powered, as a temperature change results in a voltage change. The NFJ sensor measures temperature using an open-circuit voltage between two junctions, with a sensitivity of ~1–10 mV K^{-1}; the thermocouple measures it using an open-circuit voltage between two dissimilar metals, with a sensitivity of ~10–100 μV K^{-1}. In addition, the NFJ sensor is based on an interfacial phenomenon, allowing it to operate without a temperature difference between the point of interest and the voltage measurement point. By contrast, the thermocouple is based on a bulk phenomenon and requires a temperature difference between these two points. When the temperature difference is fixed, continuous connection to a voltmeter causes a voltage drop in the NFJ sensor over time by discharging the junction capacitor, but maintains a constant voltage in the thermocouple. Furthermore, because the NFJ sensor is made of ionic and electronic conductors, it can be stretchable and transparent, unlike the thermocouple, which is rigid and opaque.

NFJ temperature sensors have distinct benefits over two other types of thermometers, the resistive temperature detector and the thermistor. Similar to thermocouples, conventional versions of the resistive temperature detector and the thermistor are stiff, unstretchable and opaque, because they are made of metal and semiconductor, respectively. Neither the resistive temperature detector nor the thermistor is self-powered, unlike the NFJ sensor. Stretchable resistive thermometers are under development[46–50], but they still are not self-powered.

Chemical sensing

Compared with pressure, acoustic and temperature sensing, the challenge of chemical sensing is that numerous species of chemicals exist in the world. Detection of a single analyte in a complex background is important to food safety and health but has been shown to be difficult. The difficulty comes from the similarity between analytes, design of analyte-specific chemistries and calibration for each analyte. Established NFJ chemical sensors include electrolyte–insulator–semiconductor devices[51,52] (Fig. 6a) and light addressable potentiometric sensors[53,54] (Fig. 6b). In an electrolyte–insulator–semiconductor device, when an analyte in the electrolyte adsorbs at the electrolyte–insulator interface, the impedance of the semiconductor channel changes and the current flowing through the channel changes at the same applied gate voltage. The device detects the adsorption of chemicals by measuring the voltage–current curve. In a light addressable potentiometric sensor, an analyte in the electrolyte adsorbs at the electrolyte–insulator interface and the photocurrent changes at the same applied voltage. This sensor detects the adsorption of chemicals by measuring the voltage–photocurrent curve. In addition, capacitive NFJ chemical sensors have also been demonstrated[55].

A self-powered approach to chemical sensing by measuring voltage across an NFJ was described in 2022 (ref. 56). When a sensing electrode coated with receptors contacts an electrolyte, an analyte in the electrolyte adsorbs at the junction and generates a voltage (Fig. 6c). Measurement of the voltage gives the concentration of the analyte. For active electrodes, a thin layer of dielectric is needed to retard electrochemical reactions and to serve as a substrate to anchor receptors. The dielectric also provides enormous design space for selective chemical sensing with high sensitivity via diverse chemistries. Several species of metal ions and organic molecules can be detected.

In this self-powered NFJ chemical sensor[56], various metals (such as aluminium, copper, gold, platinum and iron) are used as the sensing electrode, which is switched between an electrolyte containing an analyte and the ground. The sensor can detect Fe^{3+} at an ultralow concentration of 10^{-17} M, with a sensitivity six orders of magnitude higher than the luminol test. Selective chemical sensing of other species is achieved by grafting functionalized polymer brushes to the surface of the sensing electrode. For example, polyacrylic acid polymer chains grafted to the surface of aluminium selectively detect Ca^{2+}.

In contrast to an electrolyte–insulator–semiconductor device, which integrates the adsorption and detection of analytes, the self-powered NFJ sensor (Fig. 6c) separates these processes. This separation allows the sensing electrode to be made from arbitrary materials without requiring a microelectronic fabrication facility and enables rapid prototyping of receptor–analyte pairs. Furthermore, a multiplex NFJ chemical sensor can be designed to simultaneously detect multiple analytes. Proof-of-concept wearable sensing, selective sensing and detection of biological tissues have already been demonstrated[56], suggesting that the NFJ chemical sensor may find applications in wearable, implantable and biodegradable devices.

An *RC* circuit has been developed for accurate measurement of the voltage across the junction[56]. A grounded counter electrode is immersed in an electrolyte and a reference junction is formed. A sensing electrode is in series with a charge amplifier, a capacitor of capacitance C, a resistor of resistance R and the grounded counter electrode. The sensing electrode is cleaned and switched between the ground and the electrolyte. When the sensing electrode contacts the electrolyte, the voltage across the sensing junction Φ_s is generated. The charge on the capacitor is a function of time t as $q(t) = Q_{eq}[1-\exp(-t/RC)]$, in which Q_{eq} is the equilibrium charge on the capacitor. The equilibrium charge Q_{eq} gives the voltage across the sensing junction Φ_s by $\Phi_s = Q_{eq}/C$.

In principle, the charge q can also be measured using an ammeter. Consider the sensing junction and the reference junction connected by an ammeter, a resistor of resistance R and a capacitor of capacitance C. The voltage across the reference junction is held constant, and the voltage across the sensing junction changes in response to the adsorption of an analyte. The ammeter records a current as a function of time. Take the simplest case of a voltage step as an example. The ammeter detects the flow of a non-faradaic current, which decays exponentially with a time constant RC. After measuring the current–time curve, an integration gives the charge on the capacitor C.

Finally, we discuss and compare several internal timescales. Adsorption and diffusion of ions set up an equilibrium junction. Time of adsorption is typically in a range between 10^{-15} s and 10^{-9} s (refs. 57,58). Time of diffusion is determined by the diffusivity of ions and the thickness of the ionic atmosphere (the Debye length). Taking the diffusivity of ions $D_i \sim 10^{-9}$ m^2 s^{-1} and the Debye length $L \sim 10^{-9}$ m, we estimate the time of diffusion of ions $t_i \sim L^2/D_i \sim 10^{-9}$ s. To accurately measure the charge, RC needs to be large compared with the time of adsorption and diffusion. Consequently, the response time of the NFJ chemical sensor is limited by the response time of electric instruments (for example, the charge amplifier) and not by the adsorption and diffusion of ions.

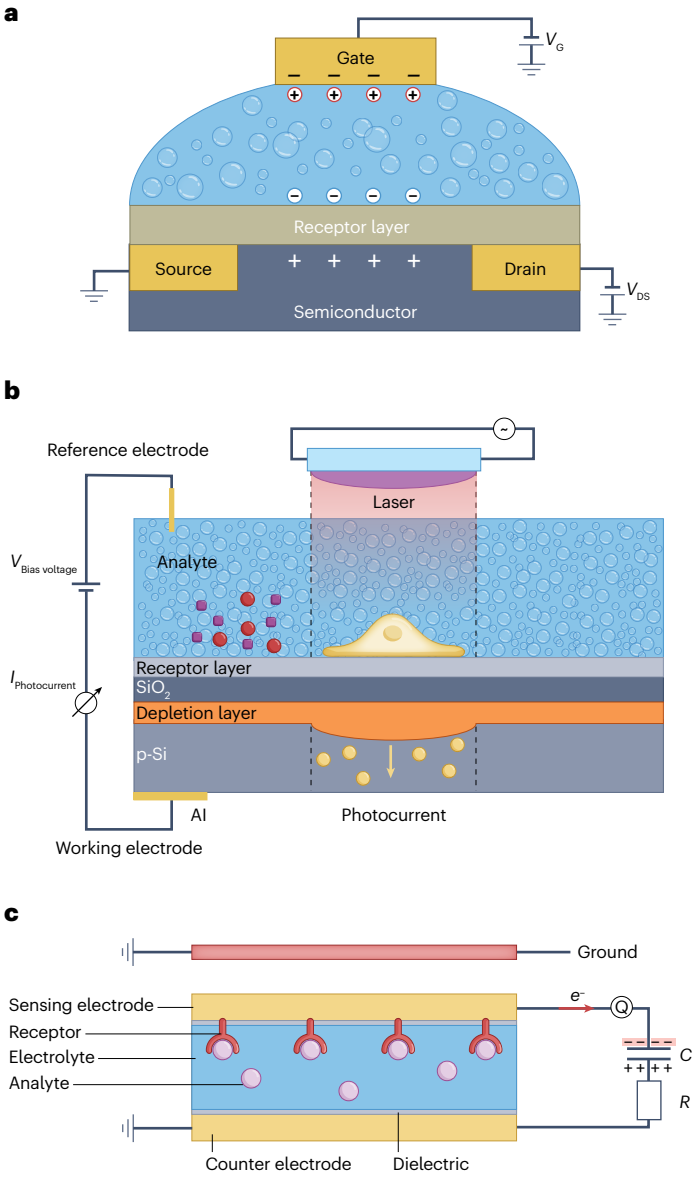

Fig. 6 | Non-faradaic junction chemical sensing. a, Electrolyte–insulator–semiconductor device[52]. The adsorption of an analyte at the receptor layer changes the impedance of the semiconductor channel and the current flowing through the channel at a given gate voltage. **b**, Light addressable potentiometric sensor[54]. The adsorption of an analyte at the receptor layer changes the impedance of the semiconductor channel and the photocurrent at a given voltage. **c**, Chemical sensor by voltage across a junction[56]. An electrolyte and two electrodes form a sensing junction and a reference junction. A charge amplifier, a capacitor *C* and a resistor *R* are connected between the sensing junction and reference junction to measure the voltage across the sensing junction. Panel **a** adapted with permission from ref. 52, Wiley. Panel **b** reprinted with permission from ref. 54, Elsevier. Panel **c** reprinted from ref. 56, CC BY 4.0.

Outlook

We now highlight the challenges and opportunities in the development of NFJ sensing.

Characterization of non-faradaic junctions

NFJs are mainly characterized by properties such as junction voltage, interfacial charge, junction capacitance and surface tension[14,192]. These macroscopic properties are determined by microscopic structures, whose characterization remains challenging. Synchrotron X-ray techniques, such as X-ray standing waves, X-ray absorption spectroscopy and X-ray photoelectron spectroscopy, have been used to investigate the ionic concentrations and electric field of NFJs[193–195]. Because the junctions are affected by a large number of variables, including concentration of each ionic species, solvent, electronic conductor, temperature, pressure, voltage and the chemistry of the interface, a full characterization of a given junction by experiments alone is an enormous task. Consequently, NFJs provide a rich platform for interdisciplinary studies using experiments, simulations and machine learning.

Self-powered non-faradaic junction sensors

Although we have described self-powered NFJ temperature and chemical sensors, existing NFJ pressure and acoustic sensors operate by measurement of capacitance. In principle, NFJ sensors of all signals can be made self-powered. For example, as the voltage across an NFJ is independent of the junction area, a change in junction capacitance by environmental signals can cause a change in charge on the electrode. Such a change in charge can be measured by a charge amplifier, and the sensor can be self-powered.

Self-cleaning non-faradaic junction sensors

By design, an NFJ chemical sensor is exposed to the environment. After some use, the junction may become contaminated by various species of molecules that affect the calibration of the junction. This contamination limits the use of sensor to a short time. Any strategy to clean or self-clean the sensors is desirable.

Multiplex sensing

In chemical sensing, many analytes might exist in a solution. A single measurement of voltage is not precise enough to detect the concentration of each analyte. One multiplexing strategy is to use an array of NFJs of various chemistries to measure multiple voltages. Each voltage is a function of the concentrations of many analytes. Collectively, the measurements determine a map between the space of concentrations and the space of voltages. This map is typically nonlinear and can be used to determine the concentration of every analyte. Such multiplex sensing strategies could be extended to include signals other than chemicals, such as temperature, pressure and stretch.

Electrolyte–electrolyte junction sensing

This Review has focused on electrode–electrolyte junctions. However, charges can adsorb at an electrolyte–electrolyte junction. The adsorbed charges will stabilize an ionic atmosphere in the electrolytes. Such a junction can also be used to develop fully ionic sensors, which mimic junctions between neurons. In particular, a junction between two types of polyelectrolytes, one carrying positive mobile ions and the other carrying negative mobile ions, functions like a semiconductor p–n junction. A few devices along these lines have been demonstrated[117,119,131].

Additive manufacturing

In principle, NFJ sensors can be made small and have arbitrary shapes, enabling sensing arrays that can map the distribution of diverse environmental signals in complex engineering structures and biological systems. However, fabrication of such NFJ sensors with unusual

geometries and structures is challenging. Additive manufacturing technologies have become highly developed for various materials and structures[161,196,197], offering potential approaches to large-scale fabrication of NFJ sensors and their arrays.

Bioelectronics

The rapid development of soft materials provides enormous flexibility in choosing electronic and ionic conductors to achieve transparency, stretchability, softness and degradability. NFJ sensors self-energize or operate at low voltage, which can serve as bioelectronic interfaces with neurons and other cells. In addition, the emerging use of soft, porous, biocompatible electronic and ionic conductors can substantially enhance the sensitivity of NFJ sensors to create robust interfaces with biological systems.

Materials

To ensure that the junction of an ionic conductor and an electronic conductor is non-faradaic, ionic and electronic conductors must be chosen such that ions and electrons do not react electrochemically. To fulfil challenging requirements in emerging applications, such as wearable devices and soft robotics, materials for each side of the junction need to be soft, stretchable, transparent and degradable.

Electronic conductor

Ideally polarizable electrodes, at which ions and electrons do not cross the junction regardless of the applied voltage, are good candidates for avoiding electrochemical reactions. Even though no such electrode exists over the entire range of voltage, many junctions are non-faradaic within ranges of voltage, called electrochemical windows. For example, the junction between mercury and deaerated potassium chloride solution is non-faradaic within a voltage range of about 2 V (ref. 14).

Most of the sensors described in this Review use metallic conductors. Inert metallic conductors, such as gold, platinum and silver, are effective at avoiding electrochemical reactions in junctions where no voltage is applied. Some active metals, such as aluminium and titanium, are passivated by a thin and dense layer of native oxide that retards electrochemical reactions and enables stable operation of NFJ sensors[45,56,59]. In principle, high entropy alloys with designable microstructures and properties[60–63] can also be used as electrodes for NFJ sensors with high sensitivity, selectivity and stability.

Carbon — including graphite, carbon grease, carbon nanotubes and graphene — is another widely used family of electronic conductors. Carbon electrodes with a high ratio of interface area to volume have been widely used in supercapacitors, actuators and sensors[64–67]. The interface between carbon and electrolyte can form an NFJ, and a large area-to-volume ratio in the carbon electrode enhances the sensitivity of NFJ sensors.

Conductive polymer typically comprises a soft elastic polymer matrix filled with conductive particles or wires[68–70]. In particular, conductive polymer hydrogel electrodes with porous structures have been used to increase junction capacitance for high-fidelity ion-electron transduction[71,72]. Such electrodes enhance the sensitivity of NFJ sensors, while making them soft and stretchable.

Semiconductors have also been used as electrodes to develop NFJ sensors. As mentioned earlier, a well-established approach to chemical sensing, the electrolyte–insulator–semiconductor device[51,52], relies on the NFJ between a semiconductor and an ionic conductor.

To make electronic conductors stretchable for emerging applications such as wearable sensing, soft robotics and stretchable bioelectronics, strategies have been developed at both geometric and material levels. Geometric designs are globally soft, but locally hard; they are stretchable by virtue of their overall shape, not the intrinsic material. Examples include serpentine metallic wires[15,73–75], metallic nanomeshes[76,77] and metallic nanowires[78,79]. Stretchable materials, including conductive polymers[68,80] and organic semiconductors[81,82], are globally soft; they are stretchable by virtue of their intrinsic material design. A common approach to producing stretchable carbon-based conductors is to disperse carbon fillers into an elastomeric matrix, forming a composite[69,83–85]. Inks of carbon (such as carbon nanotubes and graphene) can also be printed to an elastomer surface[86–90]. Transparent electronic conductors are desired for soft optical devices, such as stretchable displays. Indium tin oxide is a well-known transparent electronic conductor, but is brittle and unstretchable. In general, it is difficult to have a stretchable and transparent electronic conductor. Progress in stretchable and transparent electronic conductors has been made and several reviews are available[91–94].

Ionic conductor

Ionic conductors are a broad class of materials that include liquid electrolytes, hydrogels, ionogels and polyelectrolytes. This diversity provides enormous flexibility in designing NFJ sensors with various attributes, such as transparency, stretchability, softness and degradability. Many ionic conductors contain water. Water dissolves many other molecules and allows them to migrate freely, enabling ionic conductors to mimic the function of biological tissues. The most well-known ionic conductor is salty water, or electrolytic solution in general. Inorganic superionic conductors are also being developed for solid-state batteries[95].

Despite most ionic conductors being a liquid medium, many devices require solid-like ionic conductors. Hydrogels, polymer networks that contain a large amount of water, fit this role[13]. Despite their high water content, hydrogels retain a solid-like structure that can be designed to be stretchable and transparent. Although they have been developed since the 1960s for broad applications[96] such as contact lenses[97], superabsorbent diapers[98], drug delivery[99,100] and tissue replacement[101], the past decade has seen rapid development of an emerging field in which hydrogels serve as ionic conductors: hydrogel ionotronics[2,59,102–104]. Hydrogel ionotronics refers to a class of devices relying on both mobile ions and mobile electrons. Examples of these devices include transparent loudspeakers[13], artificial muscles[105,106], artificial axons[107,108], artificial skins[109,110], stretchable displays[111–113], soft power sources[114] and piezoionic sensors[115]. In many hydrogel-based ionic conductors, the polymer network is neutral, and ions of both polarities are mobile in water. Polyelectrolyte hydrogels, meanwhile, have a charged polymer network, and only ions of one polarity are mobile in water. The junctions between polyelectrolyte hydrogels with mobile ions of opposite polarities have been used to develop ionic diodes and ionic logic gates[116–119].

However, the water in hydrogels evaporates in open-air applications, which can dry out the ionic conductor. Ionic liquids are liquid-state salts, many of which are non-volatile. Ionogels, which are polymer networks containing an ionic liquid rather than water, have been extensively developed as non-volatile ionic conductors[120–123]. Similarly, organogels, aggregates of polymers and organic solvent, can be used for the same purpose[124–127]. Stretchable and transparent hydrogel-based, ionogel-based and organogel-based ionic conductors are discussed in more detail elsewhere[128–130].

A liquid-free stretchable ionic conductor — called an ionoelastomer — has been developed over the past few years[41,131–133]. In these conductors, one species of charge is fixed to the polymer chains, whereas the other species of charge is mobile, so the ionoelastomer functions as an ionic semiconductor. Stretchable ionic diodes and ionic transistors have been developed using the junctions between two ionoelastomers, namely, ionic double layers[131], as the doping concentration of ionoelastomers can be easily varied by copolymerization. However, no NFJ sensor using a junction of two ionic conductors has been demonstrated.

Nafion, a thermoplastic fluoropolymer with ionic channels, is a common ionic conductor in fuel cells, because it is mechanically and chemically stable. Nafion has also been widely used as the ionomer in ionic polymer–metal composite actuators and sensors[134–136]. An ionic polymer–metal composite detects mechanical signals, such as pressure and bending, by causing a flux of ions in the electrolyte, which generates a voltage between the two metal electrodes. Applications of such inorganic solid-state ionic conductors in NFJ sensors are full of opportunities[137].

Dynamic polymer networks are good material candidates for degradable and self-healing NFJ sensors, because they are reprocessable, recyclable, reshapable and weldable[138–141]. The synergy of mechanics and chemistry enables dynamic designs with desirable properties[142–144]. As a step towards this goal, ionogels of dynamic polymer networks have been developed for stretchable, healable, weldable ionotronics[145].

Dielectric

A thin layer of dielectric between an ionic conductor and an electronic conductor is able to retard any electrochemical reactions and can also serve as a substrate for functional groups to enhance the sensitivity. A familiar example is the native oxide on aluminium[146,147], which can be as thin as a few monolayers and has on its surface hydroxyl groups that can enhance the adsorption of ions and thus the sensitivity of the sensor. Even though aluminium is susceptible to electrochemical corrosion, the dense native oxide enables aluminium to be widely used in everyday life. It has been shown that a thin dielectric layer between an electrolyte and an electrode can improve sensors by stabilizing the junction and broaden the scope of usable ionic and electronic conductors[45,56]. To maintain the functionality of some devices, the dielectric needs to be thin compared with the Debye length. The dielectric layer also needs to be thick enough to be an effective barrier for tunnelling of electrons and diffusion of ions.

A dielectric-coated electrode provides enormous space for chemical design to meet requirements for applications such as sensitive and stable temperature sensing[45] and selective chemical sensing[56]. A polyelectrolyte polymer brush, namely, molecular Velcro, has also been developed[148] and can serve as a substrate to anchor functional groups.

A family of soft dielectrics is dielectric elastomer, which in the literature refers to any material that serves both as an elastomer and as a dielectric[149]. Examples include 3 M VHB, silicone rubber and polyurethane. Dielectric elastomers have been widely used in stretchable electronic and ionotronic devices, such as in soft electric actuators that mimic the function of muscles[13,150], and their mechanical and physical principles have been extensively studied[149,151–153]. When an electric field is applied to a dielectric elastomer through two soft electrodes (for example, carbon grease and hydrogel), the area of the dielectric elastomer increases and its thickness decreases. As mentioned earlier, when the thickness of dielectric elastomer is small compared with the Debye length, the dielectric elastomer can also be used as a thin dielectric layer in NFJ sensors to retard electrochemical reactions and to serve as substrates for functional groups. Such NFJ sensors remain less explored and are promising in making fully soft devices.

Dielectrics are commonly treated as good electric insulators and seals in broad applications. However, one study has shown that impedance of dielectric elastomers in the physiological environment decreases over time[154]. In other words, ions diffuse into dielectric elastomers with different diffusivities. These findings call for further study of diffusion of ions in dielectrics.

Mechanical properties

The mechanical behaviour of electronic conductors, ionic conductors and dielectrics is characterized by a large number of properties, including stiffness, strength, stretchability, toughness and fatigue threshold, among others. Ionic conductors are newer materials compared with electronic conductors and dielectrics, so proportionally more research has been dedicated to their mechanical properties over the past 20 years. The superb stiffness, toughness, strength, stretchability, adhesion, fatigue resistance and lubrication of hydrogels in particular have received a lot of attention[155–161]. For example, the relationship between synthesis and properties of elastic hydrogels has been studied, with emphasis on the effects of crosslinks and entanglements under monotonic load[162] and cyclic load[163]. Reviews on design principle of hydrogels[138,164] and an ongoing series of papers on polyacrylamide hydrogels[162,165–169] are available for details.

Adhesion among the electronic conductor, ionic conductor and dielectric components is important for stretchable NFJ sensors. Depending on the application, such as wearable and implantable sensing, adhesion that is fast, strong, tough, stable, reversible, detachable, biocompatible, biodegradable, waterproof and/or conductive can be desirable[148,170–174]. To ensure the functionality of the devices, the adhesion should not affect the electrical properties of the junction. Among the materials used in NFJ sensors, it is most challenging to realize tough adhesion in hydrogel-based ionic conductors owing to the abundance of water, which does not carry and transfer load. Achieving tough hydrogel adhesion requires supramolecular synergy of the chemistry of bonds, the mechanics of dissipation and the topology of connection[175]. Examples of approaches to tough hydrogel adhesion include covalent adhesion[171,172], non-covalent adhesion[148,170] and topological adhesion[173,174].

The quality of adhesion among the electronic conductor, ionic conductor and dielectric components affects the performance and robustness of stretchable NFJ sensors. Adhesion is characterized by mechanical tests, such as the probe-pull test, lap shear test and peel test. Among them, the lap shear test has been used to measure adhesion strength and adhesion toughness. For adhesion of hydrogel-based ionic conductors, the distinction and applicability of the two types of lap shear measurement have been identified[176,177].

Long-term stability and reliability of NFJ sensors rely on the fatigue resistance of their electronic conductors, ionic conductors and dielectrics under cyclic loads. Fatigue causes nucleation and growth of cracks in materials and subsequent degradation of mechanical properties. Studies on fatigue of electronic conductors and dielectrics, such as metals, plastics and elastomers, have been extensive[178–181], whereas studies on fatigue of ionic conductors, hydrogels in particular, are more recent[182,183]. A general principle for materials to resist fatigue has been proposed: deconcentrate stress elastically[184]. On the basis of that principle, fatigue-resistant soft materials have been realized by many forms of macrostructural and microstructural or molecular design[157–159,185–191].

Published online: 09 December 2024

References

1. Hood, L. & Price, N. *The Age of Scientific Wellness: Why the Future of Medicine is Personalized, Predictive, Data-Rich, and in Your Hands* (Harvard Univ. Press, 2023).
2. Yang, C. & Suo, Z. Hydrogel ionotronics. *Nat. Rev. Mater.* **3**, 125–142 (2018).
3. Lee, Y., Song, W. J. & Sun, J. Y. Hydrogel soft robotics. *Mater. Today Phys.* **15**, 100258 (2020).
4. Liu, X., Liu, J., Lin, S. & Zhao, X. Hydrogel machines. *Mater. Today* **36**, 102–124 (2020).
5. Herrmann, A., Haag, R. & Schedler, U. Hydrogels and their role in biosensing applications. *Adv. Healthc. Mater.* **10**, 2100062 (2021).
6. Ying, B. & Liu, X. Skin-like hydrogel devices for wearable sensing, soft robotics and beyond. *iScience* **24**, 103174 (2021).
7. Xiong, Y., Han, J., Wang, Y., Wang, Z. L. & Sun, Q. Emerging iontronic sensing: materials, mechanisms, and applications. *Research* **2022**, 9867378 (2022).
8. Xiao, K., Wan, C., Jiang, L., Chen, X. & Antonietti, M. Bioinspired ionic sensory systems: the successor of electronics. *Adv. Mater.* **32**, 2000218 (2020).
9. Steele, B. C. H. & Heinzel, A. Materials for fuel-cell technologies. *Nature* **414**, 345–352 (2001).
10. de Vasconcelos, L. S. et al. Chemomechanics of rechargeable batteries: status, theories, and perspectives. *Chem. Rev.* **122**, 13043–13107 (2022).
11. Kimmel, D. W., LeBlanc, G., Meschievitz, M. E. & Cliffel, D. E. Electrochemical sensors and biosensors. *Anal. Chem.* **84**, 685–707 (2012).
12. Choi, N.-S. et al. Challenges facing lithium batteries and electrical double-layer capacitors. *Angew. Chem. Int. Ed.* **51**, 9994–10024 (2012).
13. Keplinger, C. et al. Stretchable, transparent, ionic conductors. *Science* **341**, 984–987 (2013).
14. Bard, A. J., Faulkner, L. R., Leddy, J. & Zoski, C. G. *Electrochemical Methods: Fundamentals and Applications* Vol. 2 (Wiley, 1980).
15. Kim, D.-H. et al. Epidermal electronics. *Science* **333**, 838–843 (2011).
16. Hammock, M. L., Chortos, A., Tee, B. C. K., Tok, J. B. H. & Bao, Z. 25th Anniversary article: the evolution of electronic skin (E-Skin): a brief history, design considerations, and recent progress. *Adv. Mater.* **25**, 5997–6038 (2013).
17. Yokota, T. et al. Ultraflexible organic photonic skin. *Sci. Adv.* **2**, e1501856 (2016).
18. Yang, J. C. et al. Electronic skin: recent progress and future prospects for skin-attachable devices for health monitoring, robotics, and prosthetics. *Adv. Mater.* **31**, 1904765 (2019).
19. Liu, S., Rao, Y., Jang, H., Tan, P. & Lu, N. Strategies for body-conformable electronics. *Matter* **5**, 1104–1136 (2022).
20. Rogers, J. A., Someya, T. & Huang, Y. Materials and mechanics for stretchable electronics. *Science* **327**, 1603–1607 (2010).
21. Zhang, S. et al. Stretchable electrets: nanoparticle–elastomer composites. *Nano Lett.* **20**, 4580–4587 (2020).
22. Luo, Y. et al. Technology roadmap for flexible sensors. *ACS Nano* **17**, 5211–5295 (2023).
23. Elgrishi, N. et al. A practical beginner's guide to cyclic voltammetry. *J. Chem. Educ.* **95**, 197–206 (2018).
24. Nie, B., Xing, S., Brandt, J. D. & Pan, T. Droplet-based interfacial capacitive sensing. *Lab Chip* **12**, 1110–1118 (2012).
25. Nie, B., Li, R., Brandt, J. D. & Pan, T. Iontronic microdroplet array for flexible ultrasensitive tactile sensing. *Lab Chip* **14**, 1107–1116, (2014).
26. Nie, B., Li, R., Cao, J., Brandt, J. D. & Pan, T. Flexible transparent iontronic film for interfacial capacitive pressure sensing. *Adv. Mater.* **27**, 6055–6062 (2015).
27. Zhu, Z., Li, R. & Pan, T. Imperceptible epidermal–iontronic interface for wearable sensing. *Adv. Mater.* **30**, 1705122 (2018).
28. Heikenfeld, J. et al. Wearable sensors: modalities, challenges, and prospects. *Lab Chip* **18**, 217–248 (2018).
29. Chang, Y. et al. First decade of interfacial iontronic sensing: from droplet sensors to artificial skins. *Adv. Mater.* **33**, 2003464 (2021).
30. Lu, P. et al. Iontronic pressure sensor with high sensitivity and linear response over a wide pressure range based on soft micropillared electrodes. *Sci. Bull.* **66**, 1091–1100 (2021).
31. Zhu, P. et al. Skin–electrode iontronic interface for mechanosensing. *Nat. Commun.* **12**, 4731 (2021).
32. Yang, R. et al. Iontronic pressure sensor with high sensitivity over ultra-broad linear range enabled by laser-induced gradient micro-pyramids. *Nat. Commun.* **14**, 2907 (2023).
33. Cho, S. H. et al. Micropatterned pyramidal ionic gels for sensing broad-range pressures with high sensitivity. *ACS Appl. Mater. Interfaces* **9**, 10128–10135 (2017).
34. Li, R. et al. Supercapacitive iontronic nanofabric sensing. *Adv. Mater.* **29**, 1700253 (2017).
35. Chhetry, A., Kim, J., Yoon, H. & Park, J. Y. Ultrasensitive interfacial capacitive pressure sensor based on a randomly distributed microstructured iontronic film for wearable applications. *ACS Appl. Mater. Interfaces* **11**, 3438–3449 (2019).
36. Bai, N. et al. Graded intrafillable architecture-based iontronic pressure sensor with ultra-broad-range high sensitivity. *Nat. Commun.* **11**, 209 (2020).
37. Xiao, Y. et al. Multilayer double-sided microstructured flexible iontronic pressure sensor with a record-wide linear working range. *ACS Sens.* **6**, 1785–1795 (2021).
38. Bai, N. et al. Graded interlocks for iontronic pressure sensors with high sensitivity and high linearity over a broad range. *ACS Nano* **16**, 4338–4347 (2022).
39. Jin, M. L. et al. An ultrasensitive, visco-poroelastic artificial mechanotransducer skin inspired by piezo2 protein in mammalian Merkel cells. *Adv. Mater.* **29**, 1605973 (2017).
40. Choi, D. et al. A highly sensitive tactile sensor using a pyramid-plug structure for detecting pressure, shear force, and torsion. *Adv. Mater. Technol.* **4**, 1800284 (2019).
41. Yuan, Y.-M. et al. Microstructured polyelectrolyte elastomer-based ionotronic sensors with high sensitivities and excellent stability for artificial skins. *Adv. Mater.* **36**, 2310429 (2024).
42. Gao, Y. et al. Hydrogel microphones for stealthy underwater listening. *Nat. Commun.* **7**, 12316 (2016).
43. Wang, M. et al. Ionogel microphones detect underwater sound with directivity and exceptional stability. *ACS Appl. Electron. Mater.* **2**, 1295–1303 (2020).
44. Li, S. et al. Gate-free hydrogel–graphene transistors as underwater microphones. *ACS Appl. Mater. Interfaces* **10**, 42573–42582 (2018).
45. Wang, Y. et al. Temperature sensing using junctions between mobile ions and mobile electrons. *Proc. Natl Acad. Sci. USA* **119**, e2117962119 (2022).
46. Webb, R. C. et al. Ultrathin conformal devices for precise and continuous thermal characterization of human skin. *Nat. Mater.* **12**, 938 (2013).
47. Yokota, T. et al. Ultraflexible, large-area, physiological temperature sensors for multipoint measurements. *Proc. Natl Acad. Sci. USA* **112**, 14533–14538 (2015).
48. Trung, T. Q., Ramasundaram, S., Hwang, B.-U. & Lee, N.-E. An all-elastomeric transparent and stretchable temperature sensor for body-attachable wearable electronics. *Adv. Mater.* **28**, 502–509 (2016).
49. Wu, J. et al. Highly stretchable and transparent thermistor based on self-healing double network hydrogel. *ACS Appl. Mater. Interfaces* **10**, 19097–19105 (2018).
50. Wu, Z. et al. Ultrasensitive, stretchable, and fast-response temperature sensors based on hydrogel films for wearable applications. *ACS Appl. Mater. Interfaces* **13**, 21854–21864 (2021).
51. Schöning, M. J. & Poghossian, A. Recent advances in biologically sensitive field-effect transistors (BioFETs). *Analyst* **127**, 1137–1151 (2002).
52. Palazzo, G. et al. Detection beyond Debye's length with an electrolyte-gated organic field-effect transistor. *Adv. Mater.* **27**, 911–916 (2015).
53. Hafeman, D. G., Parce, J. W. & McConnell, H. M. Light-addressable potentiometric sensor for biochemical systems. *Science* **240**, 1182–1185 (1988).
54. Du, L. et al. Dual functional extracellular recording using a light-addressable potentiometric sensor for bitter signal transduction. *Anal. Chim. Acta* **1022**, 106–112 (2018).
55. Liu, Y.-L. et al. Electrical double layer-based iontronic sensor for detection of electrolytes concentration. *Chin. J. Anal. Chem.* **50**, 13–19 (2022).
56. Wang, Y., Zhang, S., Bai, Y., Jia, K. & Suo, Z. Chemical sensing by interfacial voltage. *Cell Rep. Phys. Sci.* **3**, 101119 (2022).
57. Björneholm, O., Nilsson, A., Sandell, A., Hernnäs, B. & Mrtensson, N. Determination of time scales for charge-transfer screening in physisorbed molecules. *Phys. Rev. Lett.* **68**, 1892–1895 (1992).
58. Zangi, R. & Engberts, J. B. F. N. Physisorption of hydroxide ions from aqueous solution to a hydrophobic surface. *J. Am. Chem. Soc.* **127**, 2272–2276 (2005).
59. Jiang, Y. et al. Frequency-dependent electrochemical breakdown of hydrogel ionotronics. *Extrem. Mech. Lett.* **71**, 102210 (2024).
60. Zhang, Y. et al. Microstructures and properties of high-entropy alloys. *Prog. Mater. Sci.* **61**, 1–93 (2014).
61. Miracle, D. B. & Senkov, O. N. A critical review of high entropy alloys and related concepts. *Acta Mater.* **122**, 448–511 (2017).
62. George, E. P., Raabe, D. & Ritchie, R. O. High-entropy alloys. *Nat. Rev. Mater.* **4**, 515–534 (2019).
63. Kong, K., Hyun, J., Kim, Y., Kim, W. & Kim, D. Nanoporous structure synthesized by selective phase dissolution of AlCoCrFeNi high entropy alloy and its electrochemical properties as supercapacitor electrode. *J. Power Sources* **437**, 226927 (2019).
64. Lee, J. A. et al. Ultrafast charge and discharge biscrolled yarn supercapacitors for textiles and microdevices. *Nat. Commun.* **4**, 1970 (2013).
65. Baughman, R. H. et al. Carbon nanotube actuators. *Science* **284**, 1340–1344 (1999).
66. Torop, J. et al. Flexible supercapacitor-like actuator with carbide-derived carbon electrodes. *Carbon* **49**, 3113–3119 (2011).
67. Foroughi, J. et al. Knitted carbon-nanotube-sheath/spandex-core elastomeric yarns for artificial muscles and strain sensing. *ACS Nano* **10**, 9129–9135 (2016).
68. Nezakati, T., Seifalian, A., Tan, A. & Seifalian, A. M. Conductive polymers: opportunities and challenges in biomedical applications. *Chem. Rev.* **118**, 6766–6843 (2018).
69. Zhang, W., Dehghani-Sanij, A. A. & Blackburn, R. S. Carbon based conductive polymer composites. *J. Mater. Sci.* **42**, 3408–3418 (2007).
70. Kumar, D. & Sharma, R. C. Advances in conductive polymers. *Eur. Polym. J.* **34**, 1053–1060 (1998).
71. Yao, B. et al. Ultrastrong, highly conductive and capacitive hydrogel electrode for electron-ion transduction. *Matter* **5**, 4407–4424 (2022).
72. Cui, M., Zhang, C., Mo, J. & Wang, Z. A general strategy to achieve high-fidelity electron-ion transduction. *Matter* **5**, 4107–4109 (2022).
73. Lacour, S. P., Wagner, S., Huang, Z. & Suo, Z. Stretchable gold conductors on elastomeric substrates. *Appl. Phys. Lett.* **82**, 2404–2406 (2003).
74. Li, T., Huang, Z., Suo, Z., Lacour, S. P. & Wagner, S. Stretchability of thin metal films on elastomer substrates. *Appl. Phys. Lett.* **85**, 3435–3437 (2004).
75. Lacour, S. P., Jones, J., Suo, Z. & Wagner, S. Design and performance of thin metal film interconnects for skin-like electronic circuits. *IEEE Electron. Device Lett.* **25**, 179–181 (2004).
76. Guo, C. F., Sun, T., Liu, Q., Suo, Z. & Ren, Z. Highly stretchable and transparent nanomesh electrodes made by grain boundary lithography. *Nat. Commun.* **5**, 3121 (2014).
77. Guo, C. F. et al. Fatigue-free, superstretchable, transparent, and biocompatible metal electrodes. *Proc. Natl Acad. Sci. USA* **112**, 12332–12337 (2015).

78. Wu, Y., Xiang, J., Yang, C., Lu, W. & Lieber, C. M. Single-crystal metallic nanowires and metal/semiconductor nanowire heterostructures. *Nature* **430**, 61–65 (2004).
79. Won, P. et al. Stretchable and transparent kirigami conductor of nanowire percolation network for electronic skin applications. *Nano Lett.* **19**, 6087–6096 (2019).
80. Wang, Y. et al. A highly stretchable, transparent, and conductive polymer. *Sci. Adv.* **3**, e1602076 (2017).
81. Root, S. E., Savagatrup, S., Printz, A. D., Rodriquez, D. & Lipomi, D. J. Mechanical properties of organic semiconductors for stretchable, highly flexible, and mechanically robust electronics. *Chem. Rev.* **117**, 6467–6499 (2017).
82. O'Connor, T. F., Rajan, K. M., Printz, A. D. & Lipomi, D. J. Toward organic electronics with properties inspired by biological tissue. *J. Mater. Chem. B* **3**, 4947–4952 (2015).
83. Zu, M., Li, Q., Wang, G., Byun, J.-H. & Chou, T.-W. Carbon nanotube fiber based stretchable conductor. *Adv. Funct. Mater.* **23**, 789–793 (2013).
84. Song, P., Song, J. & Zhang, Y. Stretchable conductor based on carbon nanotube/carbon black silicone rubber nanocomposites with highly mechanical, electrical properties and strain sensitivity. *Compos. B Eng.* **191**, 107979 (2020).
85. Xu, F., Wang, X., Zhu, Y. & Zhu, Y. Wavy ribbons of carbon nanotubes for stretchable conductors. *Adv. Funct. Mater.* **22**, 1279–1283 (2012).
86. Song, C. et al. A printed highly stretchable supercapacitor by a combination of carbon ink and polymer network. *Extrem. Mech. Lett.* **49**, 101459 (2021).
87. Chun, K.-Y. et al. Highly conductive, printable and stretchable composite films of carbon nanotubes and silver. *Nat. Nanotechnol.* **5**, 853–857 (2010).
88. Li, D., Lai, W.-Y., Zhang, Y.-Z. & Huang, W. Printable transparent conductive films for flexible electronics. *Adv. Mater.* **30**, 1704738 (2018).
89. Huang, Q. & Zhu, Y. Printing conductive nanomaterials for flexible and stretchable electronics: a review of materials, processes, and applications. *Adv. Mater. Technol.* **4**, 1800546 (2019).
90. Rosset, S. & Shea, H. R. Flexible and stretchable electrodes for dielectric elastomer actuators. *Appl. Phys. A* **110**, 281–307 (2013).
91. McCoul, D., Hu, W., Gao, M., Mehta, V. & Pei, Q. Recent advances in stretchable and transparent electronic materials. *Adv. Electron. Mater.* **2**, 1500407 (2016).
92. Matsuhisa, N., Chen, X., Bao, Z. & Someya, T. Materials and structural designs of stretchable conductors. *Chem. Soc. Rev.* **48**, 2946–2966 (2019).
93. Chen, Z. H., Fang, R., Li, W. & Guan, J. Stretchable transparent conductors: from micro/macromechanics to applications. *Adv. Mater.* **31**, 1900756 (2019).
94. Kim, K., Park, Y.-G., Hyun, B. G., Choi, M. & Park, J.-U. Recent advances in transparent electronics with stretchable forms. *Adv. Mater.* **31**, 1804690 (2019).
95. Li, Y. et al. A lithium superionic conductor for millimeter-thick battery electrode. *Science* **381**, 50–53 (2023).
96. Buwalda, S. J. et al. Hydrogels in a historical perspective: from simple networks to smart materials. *J. Control. Rel.* **190**, 254–273 (2014).
97. Wichterle, O. & LÍM, D. Hydrophilic gels for biological use. *Nature* **185**, 117–118 (1960).
98. Masuda, F. in *Superabsorbent Polymers* 573, *ACS Symposium Series* 88–98 (American Chemical Society, 1994).
99. Langer, R. Drug delivery and targeting. *Nature* **392**, 5–10 (1998).
100. Li, J. & Mooney, D. J. Designing hydrogels for controlled drug delivery. *Nat. Rev. Mater.* **1**, 16071 (2016).
101. Naahidi, S. et al. Biocompatibility of hydrogel-based scaffolds for tissue engineering applications. *Biotechnol. Adv.* **35**, 530–544 (2017).
102. Wan, C., Xiao, K., Angelin, A., Antonietti, M. & Chen, X. The rise of bioinspired ionotronics. *Adv. Intell. Syst.* **1**, 1900073 (2019).
103. Lee, H.-R., Kim, C.-C. & Sun, J.-Y. Stretchable ionics — a promising candidate for upcoming wearable devices. *Adv. Mater.* **30**, 1704403 (2018).
104. Jia, K., Li, X. & Wang, Y. Electrochemical breakdown in hydrogel ionotronic devices. *Soft Matter* **17**, 834–839 (2021).
105. Kellaris, N., Gopaluni Venkata, V., Smith, G. M., Mitchell, S. K. & Keplinger, C. Peano-HASEL actuators: muscle-mimetic, electrohydraulic transducers that linearly contract on activation. *Sci. Robot.* **3**, eaar3276 (2018).
106. Acome, E. et al. Hydraulically amplified self-healing electrostatic actuators with muscle-like performance. *Science* **359**, 61–65 (2018).
107. Yang, C. H. et al. Ionic cable. *Extrem. Mech. Lett.* **3**, 59–65 (2015).
108. Wang, Y., Xie, S., Bai, Y., Suo, Z. & Jia, K. Transduction between magnets and ions. *Mater. Horiz.* **8**, 1959–1965 (2021).
109. Sun, J.-Y., Keplinger, C., Whitesides, G. M. & Suo, Z. Ionic skin. *Adv. Mater.* **26**, 7608–7614 (2014).
110. Kim, C.-C., Lee, H.-H., Oh, K. H. & Sun, J.-Y. Highly stretchable, transparent ionic touch panel. *Science* **353**, 682–687 (2016).
111. Yang, C. H., Chen, B., Zhou, J., Chen, Y. M. & Suo, Z. Electroluminescence of giant stretchability. *Adv. Mater.* **28**, 4480–4484 (2016).
112. Larson, C. et al. Highly stretchable electroluminescent skin for optical signaling and tactile sensing. *Science* **351**, 1071–1074 (2016).
113. Yang, C. et al. Ionotronic luminescent fibers, fabrics, and other configurations. *Adv. Mater.* **32**, 2005545 (2020).
114. Schroeder, T. B. H. et al. An electric-eel-inspired soft power source from stacked hydrogels. *Nature* **552**, 214–218 (2017).
115. Dobashi, Y. et al. Piezoionic mechanoreceptors: force-induced current generation in hydrogels. *Science* **376**, 502–507 (2022).
116. Cayre, O. J., Chang, S. T. & Velev, O. D. Polyelectrolyte diode: nonlinear current response of a junction between aqueous ionic gels. *J. Am. Chem. Soc.* **129**, 10801–10806 (2007).
117. Lim, S.-M. et al. Ion-to-ion amplification through an open-junction ionic diode. *Proc. Natl Acad. Sci. USA* **116**, 13807–13815 (2019).
118. Lee, H.-R. et al. A stretchable ionic diode from copolyelectrolyte hydrogels with methacrylated polysaccharides. *Adv. Funct. Mater.* **29**, 1806909 (2019).
119. Wang, Y., Wang, Z., Su, Z. & Cai, S. Stretchable and transparent ionic diode and logic gates. *Extrem. Mech. Lett.* **28**, 81–86 (2019).
120. Chen, B. et al. Highly stretchable and transparent ionogels as nonvolatile conductors for dielectric elastomer transducers. *ACS Appl. Mater. Interfaces* **6**, 7840–7845 (2014).
121. Yiming, B. et al. Ambiently and mechanically stable ionogels for soft ionotronics. *Adv. Funct. Mater.* **31**, 2102773 (2021).
122. Ren, Y. et al. Ionic liquid-based click-ionogels. *Sci. Adv.* **5**, eaax0648 (2019).
123. Li, T., Wang, Y., Li, S., Liu, X. & Sun, J. Mechanically robust, elastic, and healable ionogels for highly sensitive ultra-durable ionic skins. *Adv. Mater.* **32**, 2002706 (2020).
124. Gao, Y. et al. Highly stretchable organogel ionic conductors with extreme-temperature tolerance. *Chem. Mater.* **31**, 3257–3264 (2019).
125. Zhang, L. et al. Stretchable and transparent ionogel-based heaters. *Mater. Horiz.* **9**, 1911–1920 (2022).
126. Shi, L. et al. Highly stretchable and transparent ionic conductor with novel hydrophobicity and extreme-temperature tolerance. *Research* **2020**, 2505619 (2020).
127. Zhao, Y. et al. A self-healing electrically conductive organogel composite. *Nat. Electron.* **6**, 206–215 (2023).
128. Park, J.-M., Lim, S. & Sun, J.-Y. Materials development in stretchable iontronics. *Soft Matter* **18**, 6487–6510 (2022).
129. Chen, N., Zhang, H., Li, L., Chen, R. & Guo, S. Ionogel electrolytes for high-performance lithium batteries: a review. *Adv. Energy Mater.* **8**, 1702675 (2018).
130. Kuzina, M. A., Kartsev, D. D., Stratonovich, A. V. & Levkin, P. A. Organogels versus hydrogels: advantages, challenges, and applications. *Adv. Funct. Mater.* **33**, 2301421 (2023).
131. Kim, H. J., Chen, B., Suo, Z. & Hayward, R. C. Ionoelastomer junctions between polymer networks of fixed anions and cations. *Science* **367**, 773–776 (2020).
132. Li, C. et al. Polyelectrolyte elastomer-based ionotronic sensors with multi-mode sensing capabilities via multi-material 3D printing. *Nat. Commun.* **14**, 4853 (2023).
133. Zhang, C. et al. 3D printed, solid-state conductive ionoelastomer as a generic building block for tactile applications. *Adv. Mater.* **34**, 2105996 (2022).
134. Jo, C., Pugal, D., Oh, I.-K., Kim, K. J. & Asaka, K. Recent advances in ionic polymer–metal composite actuators and their modeling and applications. *Prog. Polym. Sci.* **38**, 1037–1066 (2013).
135. Kamamichi, N., Yamakita, M., Asaka, K. & Zhi-Wei, L. A Snake-like Swimming Robot using IPMC Actuator/Sensor. in *Proceedings* 2006 *IEEE International Conference on Robotics and Automation. ICRA* 2006. 1812–1817 (IEEE, 2006).
136. Mirfakhrai, T., Madden, J. D. W. & Baughman, R. H. Polymer artificial muscles. *Mater. Today* **10**, 30–38 (2007).
137. Mauritz, K. A. & Moore, R. B. State of understanding of nafion. *Chem. Rev.* **104**, 4535–4586 (2004).
138. Zhao, X. et al. Soft materials by design: unconventional polymer networks give extreme properties. *Chem. Rev.* **121**, 4309–4372 (2021).
139. Zou, W., Dong, J., Luo, Y., Zhao, Q. & Xie, T. Dynamic covalent polymer networks: from old chemistry to modern day innovations. *Adv. Mater.* **29**, 1606100 (2017).
140. Zheng, N., Xu, Y., Zhao, Q. & Xie, T. Dynamic covalent polymer networks: a molecular platform for designing functions beyond chemical recycling and self-healing. *Chem. Rev.* **121**, 1716–1745 (2021).
141. Shi, Q., Jin, C., Chen, Z., An, L. & Wang, T. On the welding of vitrimers: chemistry, mechanics and applications. *Adv. Funct. Mater.* **33**, 2300288 (2023).
142. Shi, Q., Yu, K., Dunn, M. L., Wang, T. & Qi, H. J. Solvent assisted pressure-free surface welding and reprocessing of malleable epoxy polymers. *Macromolecules* **49**, 5527–5537 (2016).
143. Yu, K. et al. Interfacial welding of dynamic covalent network polymers. *J. Mech. Phys. Solids* **94**, 1–17 (2016).
144. An, L., Shi, Q., Jin, C., Zhao, W. & Wang, T. J. Chain diffusion based framework for modeling the welding of vitrimers. *J. Mech. Phys. Solids* **164**, 104883 (2022).
145. Bui, K. et al. Stretchable, healable, and weldable vitrimer ionogel for ionotronic applications. *Chem. Eng. J.* **474**, 145533 (2023).
146. Peri, J. B. & Hannan, R. B. Surface hydroxyl groups on Γ-alumina1. *J. Phys. Chem.* **64**, 1526–1530 (1960).
147. Tamura, H., Mita, K., Tanaka, A. & Ito, M. Mechanism of hydroxylation of metal oxide surfaces. *J. Colloid Interface Sci.* **243**, 202–207 (2001).
148. Wang, Y. et al. Instant, tough, noncovalent adhesion. *ACS Appl. Mater. Interfaces* **11**, 40749–40757 (2019).
149. Suo, Z. Theory of dielectric elastomers. *Acta Mech. Solid Sin.* **23**, 549–578 (2010).
150. Pelrine, R., Kornbluh, R., Pei, Q. & Joseph, J. High-speed electrically actuated elastomers with strain greater than 100%. *Science* **287**, 836–839 (2000).
151. Lu, T., Ma, C. & Wang, T. Mechanics of dielectric elastomer structures: a review. *Extrem. Mech. Lett.* **38**, 100752 (2020).
152. Lu, T., An, L., Li, J., Yuan, C. & Wang, T. J. Electro-mechanical coupling bifurcation and bulging propagation in a cylindrical dielectric elastomer tube. *J. Mech. Phys. Solids* **85**, 160–175 (2015).
153. An, L., Wang, F., Cheng, S., Lu, T. & Wang, T. J. Experimental investigation of the electromechanical phase transition in a dielectric elastomer tube. *Smart Mater. Struct.* **24**, 035006 (2015).

154. Le Floch, P. et al. Fundamental limits to the electrochemical impedance stability of dielectric elastomers in bioelectronics. *Nano Lett.* **20**, 224–233 (2020).
155. Gong, J. P., Katsuyama, Y., Kurokawa, T. & Osada, Y. Double-network hydrogels with extremely high mechanical strength. *Adv. Mater.* **15**, 1155–1158 (2003).
156. Sun, J.-Y. et al. Highly stretchable and tough hydrogels. *Nature* **489**, 133 (2012).
157. Kim, J., Zhang, G., Shi, M. & Suo, Z. Fracture, fatigue, and friction of polymers in which entanglements greatly outnumber cross-links. *Science* **374**, 212–216 (2021).
158. Hua, M. et al. Strong tough hydrogels via the synergy of freeze-casting and salting out. *Nature* **590**, 594–599 (2021).
159. Xiang, C. et al. Stretchable and fatigue-resistant materials. *Mater. Today* **34**, 7–16 (2020).
160. Mu, R. et al. Polymer-filled macroporous hydrogel for low friction. *Extrem. Mech. Lett.* **38**, 100742 (2020).
161. Xing, H. et al. Strong, tough, fatigue-resistant and 3D-printable hydrogel composites reinforced by aramid nanofibers. *Mater. Today* **68**, 84–95 (2023).
162. Wang, Y., Nian, G., Kim, J. & Suo, Z. Polyacrylamide hydrogels. VI. Synthesis–property relation. *J. Mech. Phys. Solids* **170**, 105099 (2023).
163. Wang, Y. & Sun, D. Relation of synthesis and fatigue property in elastic soft materials. *J. Mech. Phys. Solids* **193**, 105894 (2024).
164. Zhao, X. Multi-scale multi-mechanism design of tough hydrogels: building dissipation into stretchy networks. *Soft Matter* **10**, 672–687 (2014).
165. Yang, C., Yin, T. & Suo, Z. Polyacrylamide hydrogels. I. Network imperfection. *J. Mech. Phys. Solids* **131**, 43–55 (2019).
166. Liu, J. et al. Polyacrylamide hydrogels. II. elastic dissipater. *J. Mech. Phys. Solids* **133**, 103737 (2019).
167. Wang, Y., Yin, T. & Suo, Z. Polyacrylamide hydrogels. III. Lap shear and peel. *J. Mech. Phys. Solids* **150**, 104348 (2021).
168. Hassan, S., Kim, J. & Suo, Z. Polyacrylamide hydrogels. IV. Near-perfect elasticity and rate-dependent toughness. *J. Mech. Phys. Solids* **158**, 104675 (2022).
169. Kim, J., Yin, T. & Suo, Z. Polyacrylamide hydrogels. V. Some strands in a polymer network bear loads, but all strands contribute to swelling. *J. Mech. Phys. Solids* **168**, 105017 (2022).
170. Wang, Y., Liang, D., Suo, Z. & Jia, K. Synergy of noncovalent interlink and covalent toughener for tough hydrogel adhesion. *Extrem. Mech. Lett.* **39**, 100797 (2020).
171. Yuk, H., Zhang, T., Lin, S., Parada, G. A. & Zhao, X. Tough bonding of hydrogels to diverse non-porous surfaces. *Nat. Mater.* **15**, 190–196 (2016).
172. Yuk, H., Zhang, T., Parada, G. A., Liu, X. & Zhao, X. Skin-inspired hydrogel–elastomer hybrids with robust interfaces and functional microstructures. *Nat. Commun.* **7**, 12028 (2016).
173. Yang, J., Bai, R. & Suo, Z. Topological adhesion of wet materials. *Adv. Mater.* **30**, 1800671 (2018).
174. Gao, Y. et al. A universal strategy for tough adhesion of wet soft material. *Adv. Funct. Mater.* **30**, 2003207 (2020).
175. Yang, J., Bai, R., Chen, B. & Suo, Z. Hydrogel adhesion: a supramolecular synergy of chemistry, topology, and mechanics. *Adv. Funct. Mater.* **30**, 1901693 (2020).
176. Wang, Y., Yang, X., Nian, G. & Suo, Z. Strength and toughness of adhesion of soft materials measured in lap shear. *J. Mech. Phys. Solids* **143**, 103988 (2020).
177. Wang, Y., Nian, G., Yang, X. & Suo, Z. Lap shear of a soft and elastic adhesive. *Mech. Mater.* **158**, 103845 (2021).
178. Fleck, N. A., Kang, K. J. & Ashby, M. F. Overview no. 112: the cyclic properties of engineering materials. *Acta Metall. Mater.* **42**, 365–381 (1994).
179. Ritchie, R. O. Mechanisms of fatigue crack propagation in metals, ceramics and composites: role of crack tip shielding. *Mater. Sci. Eng. A* **103**, 15–28 (1988).
180. Suresh, S. *Fatigue of Materials* 2nd edn (Cambridge Univ. Press, 1998).
181. Mars, W. V. & Fatemi, A. Factors that affect the fatigue life of rubber: a literature survey. *Rubber Chem. Technol.* **77**, 391–412 (2004).
182. Bai, R., Yang, J. & Suo, Z. Fatigue of hydrogels. *Eur. J. Mech. A/Solids* **74**, 337–370 (2019).
183. Han, Z., Lu, Y. & Qu, S. Design of fatigue-resistant hydrogels. *Adv. Funct. Mater.* **34**, 2313498 (2024).
184. Steck, J., Kim, J., Kutsovsky, Y. & Suo, Z. Multiscale stress deconcentration amplifies fatigue resistance of rubber. *Nature* **624**, 303–308 (2023).
185. Wang, Z. et al. Stretchable materials of high toughness and low hysteresis. *Proc. Natl Acad. Sci. USA* **116**, 5967–5972 (2019).
186. Lin, S. et al. Anti-fatigue-fracture hydrogels. *Sci. Adv.* **5**, eaau8528 (2019).
187. Li, X. et al. Mesoscale bicontinuous networks in self-healing hydrogels delay fatigue fracture. *Proc. Natl Acad. Sci. USA* **117**, 7606–7612 (2020).
188. Lin, S., Liu, J., Liu, X. & Zhao, X. Muscle-like fatigue-resistant hydrogels by mechanical training. *Proc. Natl Acad. Sci. USA* **116**, 10244–10249 (2019).
189. Sun, D. et al. Enhance fracture toughness and fatigue resistance of hydrogels by reversible alignment of nanofibers. *ACS Appl. Mater. Interfaces* **14**, 49389–49397 (2022).
190. Liu, B. et al. Tough and fatigue-resistant polymer networks by crack tip softening. *Proc. Natl Acad. Sci. USA* **120**, e2217781120 (2023).
191. Yang, H., Chen, X., Sun, B., Tang, J. & Vlassak, J. J. Fracture tolerance induced by dynamic bonds in hydrogels. *J. Mech. Phys. Solids* **169**, 105083 (2022).
192. Parsons, R. The electrical double layer: recent experimental and theoretical developments. *Chem. Rev.* **90**, 813–826 (1990).
193. Favaro, M. et al. Unravelling the electrochemical double layer by direct probing of the solid/liquid interface. *Nat. Commun.* **7**, 12695 (2016).
194. Brown, M. A. et al. Determination of surface potential and electrical double-layer structure at the aqueous electrolyte–nanoparticle interface. *Phys. Rev. X* **6**, 011007 (2016).
195. Brown, M. A., Goel, A. & Abbas, Z. Effect of electrolyte concentration on the stern layer thickness at a charged interface. *Angew. Chem. Int. Ed.* **55**, 3790–3794 (2016).
196. Shi, Q. et al. Recyclable 3D printing of vitrimer epoxy. *Mater. Horiz.* **4**, 598–607 (2017).
197. Kuang, X. et al. Advances in 4D printing: materials and applications. *Adv. Funct. Mater.* **29**, 1805290 (2019).

Acknowledgements
Y.W. acknowledges the support of NSFC (12302225). K.J. acknowledges the support of NSFC (81974470). Z.S. acknowledges the support of the NSF through the Harvard University Materials Research Science and Engineering Center (DMR2011754) and the support of the Air Force Office of Scientific Research (FA9550-20-1-0397).

Author contributions
All authors contributed equally to the manuscript.

Competing interests
The authors declare no competing interests.

Additional information
Publisher's note Springer Nature remains neutral with regard to jurisdictional claims in published maps and institutional affiliations.